

The acidic domain of the endothelial membrane protein GPIHBP1 stabilizes lipoprotein lipase activity by preventing unfolding of its catalytic domain

Simon Mysling^{1,2,3}, Kristian K. Kristensen^{1,2}, Mikael Larsson⁴, Anne P. Beigneux⁴, Henrik Gårdsvoll^{1,2}, Loren G. Fong⁴, André Bensadoun⁶, Thomas J. D. Jørgensen³, Stephen G. Young^{4,5}, and Michael Ploug^{1,2,#}

¹Finsen Laboratory, Rigshospitalet, DK-2200 Copenhagen N, Denmark;

²Biotech Research and Innovation Centre (BRIC), University of Copenhagen, DK-220 Copenhagen N, Denmark;

³Department of Biochemistry and Molecular Biology, University of Southern Denmark, DK-5320 Odense M, Denmark;

⁴Department of Medicine, University of California, Los Angeles, CA 90095 USA;

⁵Department of Human Genetics, University of California, Los Angeles, CA 90095 USA;

⁶Division of Nutritional Science, Cornell University, Ithaca, NY 14853 USA

Key words: familial chylomicronemia, lipolysis, hypertriglyceridemia, hyperlipidemia, endothelial cell transporter, intrinsically disordered protein, HDX-MS, surface plasmon resonance

#Address correspondence to: Michael Ploug, Finsen Laboratory, Rigshospitalet, Ole Maaloes Vej 5, DK-2200 Copenhagen, Denmark; Tel: (45) 35456037; E-mail: m-ploug@finsenlab.dk

30

Abstract

GPIHBP1 is a glycolipid-anchored membrane protein of capillary endothelial cells that binds lipoprotein lipase (LPL) within the interstitial space and shuttles it to the capillary lumen. The LPL•GPIHBP1 complex is responsible for margination of triglyceride-rich lipoproteins along capillaries and their lipolytic processing. The current work conceptualizes a model for the GPIHBP1•LPL interaction based on biophysical measurements of purified proteins with hydrogen–deuterium exchange/mass spectrometry, surface plasmon resonance, and zero-length cross-linking. According to this model, GPIHBP1 is comprised of two functionally distinct domains: (1) an intrinsically disordered and highly acidic N-terminal domain; and (2) a folded C-terminal Ly6/uPAR (LU) domain that tethers GPIHBP1 to the cell membrane by a glycosylphosphatidylinositol moiety. We demonstrate that these domains serve different roles in regulating the kinetics of LPL binding. Importantly, the acidic domain stabilizes LPL catalytic activity by mitigating the global unfolding of LPL’s catalytic domain. This study provides a conceptual framework for understanding intravascular lipolysis and *GPIHBP1* and *LPL* mutations causing familial chylomicronemia.

Introduction

For nearly six decades, we have known that lipoprotein lipase (LPL), a triglyceride hydrolase secreted by myocytes and adipocytes, is essential for the lipolytic processing of triglyceride-rich lipoproteins (TRLs) in the bloodstream (Korn, 1955; Young and Zechner, 2013). LPL-mediated processing of TRLs occurs along the capillary lumen, and LPL is readily released from the surface of capillaries with polyanionic compounds such as heparin. LPL contains an N-terminal domain (NTD) for catalysis and a C-terminal domain (CTD) that is essential for lipid binding. LPL is active as a head-to-tail homodimer, and several lines of evidence suggest that the CTD of one LPL monomer delivers triglyceride substrates to the NTD of the partner monomer (Kobayashi et al., 2002). In the presence of certain LPL mutations (*e.g.*, mutations in the catalytic triad or mutations that prevent LPL dimerization), the processing of TRLs is markedly impaired, leading to severe hypertriglyceridemia (familial chylomicronemia) (Brahm and Hegele, 2015).

For decades, the mechanism by which LPL traversed endothelial cells to reach the luminal surface of capillaries—as well as LPL's binding site within capillaries—were enigmas (Brown et al., 2015). These uncertainties have been addressed by the discovery of a novel LPL binding protein of capillary endothelial cells, glycosylphosphatidylinositol-anchored high density lipoprotein-binding protein 1 (GPIHBP1). GPIHBP1 binds LPL within the interstitial spaces and transports LPL across endothelial cells to its site of action in the capillary lumen (Beigneux et al., 2007; Davies et al., 2010). In the absence of GPIHBP1, LPL does not reach the capillary lumen, and there is no margination of TRLs along the surface of capillaries (Goulbourne et al., 2014).

GPIHBP1 is a member of the LU (Ly6/uPAR) protein domain family, which includes CD59, SLURP1, C4.4A, TGF- β receptors, and uPAR. The hallmark of this protein family is a three-finger-fold with a defined disulfide pairing motif involving eight highly conserved cysteines (Ploug, 2003). Members of the LU domain family are widespread in the animal kingdom and occur as secreted proteins (*e.g.*, SLURP1), integral membrane proteins (TGF β receptors), and glycolipid-anchored proteins (*e.g.*, CD59, GPIHBP1, C4.4A, uPAR). During evolution, the LU domain has evolved to

serve many different purposes in mammals: GPIHBP1 transports LPL; CD59 inhibits complement activation; TGF β receptors are involved in cytokine signaling; TEX101 regulates fertility; and uPAR focuses plasminogen activation on cell surfaces. Although detailed structure–function relationships have been elucidated for a few mammalian LU domain proteins (*e.g.*, TGF β receptors, CD59, uPAR), progress in understanding the biochemistry and biophysics of protein interactions for the majority of LU domain proteins, including GPIHBP1, has lagged behind, largely because of the need for highly purified recombinant protein preparations.

In our opinion, GPIHBP1 represents one of the more intriguing mammalian LU domain proteins from both a functional and a structural point of view. First, GPIHBP1 function is tightly linked to human disease as a variety of loss-of-function mutations in GPIHBP1 have been encountered in humans with familial chylomicronemia (Beigneux et al., 2009; Buonuomo et al., 2015; Olivecrona et al., 2010; Plengpanich et al., 2014; Rios et al., 2012; Surendran et al., 2012). The majority of these disease-causing mutations impair the folding of the LU domain, leading to multimerized and dysfunctional GPIHBP1 molecules on the cell surface (Beigneux et al., 2015). In a comprehensive screen of GPIHBP1 mutants, one mutant (GPIHBP1^{W89S})* was found to have markedly impaired LPL binding despite being monomeric, suggesting that it retained native folding of its LU domain (Beigneux et al., 2011; Beigneux et al., 2015). Interestingly, several mutations in the CTD of LPL (*e.g.*, C418Y, first identified in a patient with chylomicronemia) have no effect on catalysis but abolish the ability of LPL to bind to GPIHBP1 (and thus prevent LPL transport across endothelial cells) (Gin et al., 2012; Henderson et al., 1996).

Second, GPIHBP1 is unique from a structural perspective. Among the entire LU protein family, only a very few proteins have N-terminal extensions (*e.g.*, GPIHBP1 and the spermatid marker SP-10). In the case of GPIHBP1, the N-terminal extension is highly enriched in acidic residues, with 21 of 26 consecutive amino acids in human GPIHBP1 being aspartic acid or glutamic acid. Early studies

* Amino acid numbering throughout this manuscript refers to the first residue in the mature protein.

in cell culture suggested that GPIHBP1's acidic domain is important for GPIHBP1•LPL interactions (Gin et al., 2008), but a detailed study of the functional impact of the acidic domain on LPL function has been lacking. One of the impediments to progress is that a large fraction of the GPIHBP1 produced by transfected mammalian cells is misfolded and in the form of multimers (Beigneux et al., 2015).

In the current study, we used highly purified proteins and a combination of hydrogen–deuterium exchange mass spectrometry (HDX-MS), surface plasmon resonance (SPR), zero-length cross-linking, and LPL activity assays to elucidate LPL•GPIHBP1 interactions both kinetically and dynamically. Our studies show: (1) that the kinetics of LPL•GPIHBP1 interactions are controlled by both the LU domain and the acidic domain of GPIHBP1; and (2) that the acidic domain is intrinsically disordered and is responsible for stabilizing the catalytic activity of LPL by inhibiting the inherent instability and subsequent unfolding of LPL's catalytic domain.

Results

Production and purification of recombinant soluble GPIHBP1

A secreted version of human GPIHBP1^{1–131} was produced in *Drosophila* S2 cells as a fusion protein with uPAR domain III (Figure 1—figure supplement 1). However, this protein proved to be prone to an internal cleavage after Arg³⁸ during enterokinase-mediated removal of the uPAR tag. This unexpected cleavage event markedly reduced the yields of purified GPIHBP1^{1–131}. Alignments of multiple primate GPIHBP1 sequences revealed that Arg³⁸ is not conserved during evolution. In GPIHBP1 from *Nomascus leucogenys*, which is 94% identical to human GPIHBP1, the residue corresponding to Arg³⁸ is Gly³⁸. Based on these homology considerations, we therefore expressed and purified a modified protein in which Arg³⁸ was replaced with Gly; this construct yielded high levels of pure GPIHBP1^{1–131/R38G} along with moderate amounts of a truncated GPIHBP1^{34–131/R38G}. That truncated protein was the result of an additional cleavage after Arg³³. Both GPIHBP1^{1–131} and

GPIHBP1^{34–131} (lacking the acidic domain) were purified to homogeneity by cation-exchange chromatography (Figure 1–figure supplement 2). Importantly, both proteins were monomeric with no traces of aggregation, as judged by analytical size-exclusion chromatography (Figure 1C). This homogeneity is a noteworthy achievement because earlier studies had shown that GPIHBP1 is highly susceptible to multimerization (Beigneux et al., 2015). The anomalous partitioning of GPIHBP1^{1–131} during size-exclusion chromatography is most likely a consequence of a large Stokes radius caused by the presence of an intrinsically disordered N-terminal peptide (see next section). Consistent with this assumption, GPIHBP1^{34–131}, which lacks the acidic domain, eluted with the expected hydrodynamic volume for a globular protein (Figure 1C).

Molecular model for GPIHBP1

Homology considerations identify GPIHBP1 as a glycolipid-anchored protein with a single prototypical LU domain (Figure 1A). Unlike other members of this protein family, GPIHBP1 contains an N-terminal domain with 21 acidic amino acids (Glu, Asp). We propose that the first 30–35 N-terminal residues in GPIHBP1 have a very high propensity for being an intrinsically disordered region (Figure 1B). The disordered nature of the acidic domain is supported by: (1) the atypically large hydrodynamic volume of GPIHBP1^{1–131} compared with GPIHBP1^{34–131} (Figure 1C); (2) its susceptibility to limited proteolysis after Arg³³ or Arg³⁸; and (3) by the highly dynamic nature of the acidic domain as judged by extremely rapid hydrogen–deuterium exchange rates. In hydrogen–deuterium exchange/mass spectrometry (HDX-MS) studies, we observed 100% deuterium uptake in this domain even after the shortest exposure time (10 sec) (Figure 1D and 1E), which is consistent with the predicted deuterium uptake for a disordered GPIHBP1^{1–33} peptide (87% after 1 sec and 100% after 10 sec). In the same experiment, HDX profiles of peptides within the LU domain followed the secondary structure prediction. The deuterium uptake in the isolated LU domain in GPIHBP1^{34–131} is indistinguishable from that of full-length GPIHBP1^{1–131} (Figure 1–figure supplement 3), which implies that the acidic N-terminal region has little or no effect on the structure

of GPIHBP1's LU domain.

Characterizing the GPIHBP1•LPL interaction with HDX-MS

To identify protein–protein binding interfaces and/or uncover conformational changes associated with GPIHBP1•LPL binding, we determined the hydrogen–deuterium exchange profiles for GPIHBP1, LPL, and GPIHBP1•LPL complexes. The GPIHBP1•LPL complexes were formed by incubating 5 μ M GPIHBP1 with 5 μ M LPL homodimers (LPL₂) for 15 min in 10 mM Na₂HPO₄, 150 mM NaCl (pH 7.4) at 25°C before monitoring solvent exchange after dilution into D₂O for 10, 100, or 1000 sec. We recovered 22 peptides from GPIHBP1 and 92 peptides from LPL after on-line pepsin digestion of quenched and TCEP-reduced proteins at pH 2.5, which correspond to 100% and 87% sequence coverage, respectively (Figure 1–supplement 4 and Figure 2–supplement 1).

As documented by the heat maps in Figure 1D, the conformation of the LU domain in GPIHBP1^{1–131} was less dynamic when bound to LPL. In particular, we observed markedly reduced deuterium uptake within strands D and E of GPIHBP1 when it formed a complex with LPL (Figure 1E). This shift in the dynamics likely reflects a transition to a state with increased secondary structure and/or a direct engagement in a ligand-binding interface. The fact that the HDX-MS analysis of GPIHBP1 identified β -strand D as a candidate binding interface for LPL was not entirely unexpected given that a previous mutagenesis study had shown that individual alanine replacements of Thr⁸⁵, Ser⁸⁷, or Trp⁸⁹ in β -strand D impaired LPL binding (Figure 1E) (Beigneux et al., 2011). Moreover, two missense mutations involving β -strand D have been associated with chylomicronemia in humans [*i.e.* Ser⁸⁷→Pro (Buonuomo et al., 2015) and Thr⁸⁸→Arg (Surendran et al., 2012)]. Mutating residues within strand E of GPIHBP1 had little impact on LPL binding (Beigneux et al., 2011). The reduced deuterium uptake that we recorded for strand E in the presence of LPL probably relates to a higher propensity for β -sheet formation in the setting of the GPIHBP1•LPL complex. Strand E is one of the most versatile structures in LU proteins; it can adopt a random coil (snake venom α -neurotoxins), a β -strand (uPAR domains I and II), or an α -helix (CD59, Prod1, and uPAR domain III) (Kriegbaum et

al., 2011). Interestingly, the deuterium uptake in the intrinsically disordered N-terminal acidic domain did not change with LPL binding. That finding suggests that the acidic domain either does not participate in the binding interaction or more likely that it is involved in very transient binding events with LPL (interactions that do not lead to the formation of stable hydrogen bonds).

From the same set of experiments, we also extracted data concerning the effects on LPL by comparing the differential deuterium uptake between unoccupied LPL and LPL in complex with either intact GPIHBP1¹⁻¹³¹ (Figure 2A) or its N-terminal acidic domain peptide GPIHBP1¹⁻³³ (Figure 2B). To minimize possible confounding effects from the inherent instability of unoccupied LPL, we only included deuterium uptake values for 10 and 100 sec for the three different states of LPL. Comparing these states, we identify residues 402–419 in the CTD of LPL as the most likely interaction site for the LU domain of GPIHBP1 (shown in blue in the butterfly plot in Figure 2A). This assignment is based on the fact that GPIHBP1¹⁻¹³¹, but not GPIHBP1¹⁻³³, attenuates the deuterium uptake in this particular region (Figure 2C). Two missense mutations in or close to this segment (C418Y and E421K) were identified in patients with chylomicronemia (Henderson et al., 1998; Henderson et al., 1996), and follow-up studies showed that both mutations impaired GPIHBP1 binding (Voss et al., 2011). It is possible that additional regions in the CTD of LPL are involved in GPIHBP1 binding but escaped detection in our HDX-MS experiments due to the lower level of sequence coverage for the CTD (69%) (Figure 2–figure supplement 1). The impact of the acidic domain peptide (GPIHBP1¹⁻³³) on LPL deuterium uptake was less pronounced than with intact GPIHBP1¹⁻¹³¹ (Figure 2A and 2B), consistent with a more dynamic interaction (*i.e.*, a shorter residence time of the peptide on LPL). Notwithstanding the more transient interaction, we did nevertheless observe that GPIHBP1¹⁻³³ reduced deuterium uptake in LPL peptides spanning residues 279–293 (Figure 2B), which is localized in the domain interface between the NTD and CTD of LPL (Figure 2D). It is noteworthy that this region contains one of the heparin-binding sites in LPL enriched in basic residues (Arg²⁸¹, Lys²⁸², Arg²⁸⁴) (Hata et al., 1993) and therefore represents a potential binding partner for GPIHBP1's acidic domain.

Kinetic rate constants for the interaction between GPIHBP1 and LPL

To dissect the individual contributions of the folded LU domain and the intrinsically disordered acidic domain on the binding kinetics with LPL, we developed and optimized a surface plasmon resonance assay to measure this interaction. In brief, we used a BiacoreT200™ to measure the binding kinetics between soluble, monomeric GPIHBP1 and either LPL's CTD or intact LPL that had been captured on a CM4 sensor chip with an immobilized anti-LPL monoclonal antibody, 5D2. This antibody is well suited to capture and display both LPL and the CTD in a defined orientation because it recognizes both proteins with high affinity (Chang et al., 1998).

Using this SPR setup, we found that full-length GPIHBP1^{1-131/R38G} binds the CTD of LPL with a K_D of $0.12 \pm 0.04 \mu\text{M}$, whereas GPIHBP1^{34-131/R38G} binds with a K_D of $1.41 \pm 0.76 \mu\text{M}$ (Table 1). The robustness of the assay is apparent by the repeat analyses of 250 nM GPIHBP1 at the end of each multi-cycle segment (blue curves in Figure 3A and 3C). In parallel, we analyzed the ability of soluble GPIHBP1 to bind to a CTD carrying a single amino acid substitution (C418Y). As noted earlier, the C418Y mutation is known to abolish LPL binding to GPIHBP1 (Henderson et al., 1996; Voss et al., 2011). When the LPL CTD^{C418Y} was captured on immobilized mAb 5D2 (85 RU \sim 5 fmols/mm²), it lacked the ability to bind GPIHBP1¹⁻¹³¹ or GPIHBP1³⁴⁻¹³¹, even at concentrations as high as 1 μM (Table 1). As an additional control, we tested the ability of GPIHBP1^{1-131/W89S} to bind the CTD of LPL. Earlier studies had shown that glycolipid-anchored GPIHBP1^{W89S} on the surface of transfected CHO-K1 cells has little or no capacity to bind LPL (Beigneux et al., 2011; Beigneux et al., 2015; Plengpanich et al., 2014). Consistent with those studies, the SPR measurements revealed negligible binding of GPIHBP1^{1-131/W89S} to the CTD of LPL (Figure 3B). Collectively, these data indicate that the intrinsically disordered acidic domain of GPIHBP1 has little effect on the affinity of the LPL•GPIHBP1 interaction in the absence of a functional LU domain.

Kinetic assessment of the SPR binding data reveals that the 5–10 fold difference in the equilibrium binding constants between GPIHBP1¹⁻¹³¹ and GPIHBP1³⁴⁻¹³¹ could be accounted for by

differences in their association rate constants: $k_{on} = 1.04 \times 10^6 \text{ M}^{-1}\text{s}^{-1}$ for GPIHBP1¹⁻¹³¹ *versus* a $k_{on} = 0.10 \times 10^6 \text{ M}^{-1}\text{s}^{-1}$ for GPIHBP1³⁴⁻¹³¹ (Table 1). In contrast, the stabilities of the GPIHBP1•CTD complexes with GPIHBP1¹⁻¹³¹ and GPIHBP1³⁴⁻¹³¹ were essentially identical; both displayed k_{off} values of 0.1 s^{-1} . Removal of the single N-linked glycosylation in GPIHBP1¹⁻¹³¹ had no significant impact on the kinetic rate constants (Table 1). Since these analyses were conducted with the R38G mutation in GPIHBP1 (which was introduced to optimize purification yields) we tested whether this mutation affects the binding kinetics between LPL and GPIHBP1. To liberate intact, wild-type GPIHBP1¹⁻¹³¹, we performed a partial cleavage of 7 mg RS-DIII-ent-GPIHBP1 with 0.05 U enterokinase/mg protein, which resulted in 70 % cleavage of the fusion protein. A sufficient amount of this full-length GPIHBP1¹⁻¹³¹ was purified by ion-exchange chromatography to allow subsequent kinetic analyses by SPR. The kinetics for the interactions between mAb 5D2-captured CTD or LPL and wild-type GPIHBP1¹⁻¹³¹ were similar to those measured with GPIHBP1^{1-131/R38G} (Table 1). Thus, the R38G mutation does not significantly affect the properties of the GPIHBP1 interaction with LPL.

A similar kinetic assessment for the binding of LPL homodimers by multi-cycle titration was, however, inherently challenging because the conditions required to regenerate mAb 5D2 between cycles progressively reduced the capturing capacity of the sensor chip. To minimize this confounding factor, we performed a single-cycle kinetic titration of the interaction between GPIHBP1 and full-length LPL dimers captured by mAb 5D2. To be confident that the captured LPL was in a properly folded and homodimeric state, we initially performed a kinetic titration with two LPL-specific monoclonal antibodies [mAb 4-1a, which binds within residues 5–25 in LPL (Bensadoun et al., 2014) and mAb 5D2, which binds to residues 380–400 in the CTD of LPL (Chang et al., 1998)]. As shown in Figure 4A, both antibodies bound immobilized LPL when analyzed by a single-cycle titration protocol. Calculation of their binding capacities [$R_{max} = 200 \text{ RU}$ for mAb 4-1a (1.3 fmols/mm^2) and $R_{max} = 309 \text{ RU}$ for mAb 5D2 (2.1 fmols/mm^2)] revealed molar surface-binding capacities that were similar to the surface density of the captured LPL homodimer [$R_{900sec} = 203 \text{ RU}$ (2.0 fmols/mm^2)]. Because mAb 5D2 is used as both capture and detection agent in this experiment, our data suggest

that the majority of the captured LPL on the sensor chip was in the form of homodimers.

The single-cycle kinetic titrations revealed fast k_{on} values for GPIHBP1•LPL interactions. The k_{off} values for the LPL complexes with GPIHBP1^{1–131} and GPIHBP1^{34–131} were 5-fold slower than for the corresponding CTD interaction, which indicates that GPIHBP1 forms a tighter complex with full-length LPL (Table 1, Figure 4B and 4C). To supplement the real-time binding kinetics recorded by surface plasmon resonance, we measured the equilibrium binding constants for the interaction between GPIHBP1^{1–131/R38G} and LPL in solution by microscale thermophoresis (MST) with a Monolith NT.115™ (NanoTemper Technologies GmbH). In these studies, 5 nM Alexa-647–labeled GPIHBP1^{1–131/R38G} or GPIHBP1^{34–131/R38G} were incubated with increasing concentrations of LPL₂ (10 pM to 350 nM). The binding isotherms were then calculated from the shifts in the thermophoresis of the fluorophore (Figure 5). With this experimental approach, we determined a K_D of 5.7 nM for the LPL•GPIHBP1^{1–131/R38G} interaction and a K_D of 147 nM for the GPIHBP1^{34–131/R38G} interaction. All things considered, we find that data with this solution-based assay aligns excellently with the binding affinities determined kinetically by SPR.

Global unfolding of LPL’s catalytic domain. We next used hydrogen–deuterium exchange to probe for conformational changes associated with the time-dependent decay of the catalytic activity in LPL (Osborne et al., 1985). For these studies, we incubated 5 μ M LPL₂ at 25°C for various times and then traced changes in the solvent exposure of backbone amide hydrogens with a 10-sec pulse labeling in D₂O. As illustrated in Figure 6, we observed a pronounced global unfolding of the catalytic domain in LPL as reflected by the appearance of a bimodal signature in the isotope envelopes from the majority of peptic peptides derived from this domain (colored red in Figure 6B). This finding implies that the NTD of LPL most likely enters a pre-molten globule-like state with little maintenance of secondary structure. The disordering of the catalytic triad is evident by the bimodal isotope envelope for the peptide 131–165, which encompasses active site residues Ser¹³⁴ and Asp¹⁵⁸ (Figure 6A and 6B). Of note, we also observed a time-dependent loss in both the triolein hydrolase and esterase

activities of 2 μ M LPL₂ with experimental conditions comparable to those for the HDX-MS studies (Figure 6D). Unexpectedly, the time course for the inactivation of LPL catalytic activity appeared to be approximately twice as fast as the unfolding of the catalytic NTD documented by HDX-MS. With prolonged incubations, we did observe a more complete unfolding of the NTD by HDX-MS (74% unfolded after 180 min and 90% after 240 min). Of note, no changes were observed in the deuterium uptake of the CTD in LPL during the same time frame (Figure 6B), consistent with a greater stability of that domain (Gin et al., 2012).

GPIHBP1¹⁻³³ attenuates the rate of LPL unfolding

The impact of GPIHBP1 on the spontaneous unfolding of LPL was subsequently addressed by HDX-MS. This was accomplished by incubating LPL in the presence of GPIHBP1¹⁻¹³¹, GPIHBP1¹⁻³³, or GPIHBP1³⁴⁻¹³¹ for 45 min at 25°C. We assessed the deuterium uptake after 10-sec labeling with D₂O. GPIHBP1¹⁻¹³¹ clearly inhibited LPL unfolding (Figure 6C). This protective effect was predominantly due to the acidic domain because the GPIHBP1¹⁻³³ peptide alone also attenuated LPL unfolding. A distinct but much less pronounced contribution was provided by GPIHBP1³⁴⁻¹³¹ on both unfolding rates and preservation of triolein hydrolase and esterase activity of LPL (Table 2).

Mapping the binding site for GPIHBP1¹⁻³³ on LPL

To map defined binding sites for GPIHBP1 on LPL, we used zero-length covalent cross-linking with N-ethyl-N'-[3-diethylamino)propyl]-carbodiimide (EDC), which forms an isopeptide bond by chemical condensation of carboxylates and primary amino groups that are in close spatial proximity. For these studies, we formed GPIHBP1•LPL complexes by incubating a high concentration of LPL with a twofold molar excess of GPIHBP1¹⁻¹³¹ or GPIHBP1³⁴⁻¹³¹ (to saturate binding sites on LPL). Adding 10 mM EDC efficiently cross-linked LPL•GPIHBP1¹⁻¹³¹ in a 1:1 complex, consuming the majority of the LPL (Figure 7, lanes 5 & 11). In contrast, no covalent adducts were formed in the

samples containing GPIHBP1¹⁻¹³¹ alone, LPL alone, or a mixture of LPL and GPIHBP1³⁴⁻¹³¹ (Figure 7, lanes 3, 4, 6 & 10). Adding EDC to LPL in the presence of a 10-fold molar excess of GPIHBP1¹⁻³³ also led to the formation of a 1:1 complex with no evidence of higher-order adducts (Figure 7, lane 9). These studies imply that each LPL molecule interacts with only a single acidic domain peptide.

To identify the specific cross-linked sites responsible for the formation of the covalent LPL•GPIHBP1 adduct, we performed an in-gel trypsin digestion of the complex that had been separated by SDS-PAGE (Figure 7, lane 5). The extracted tryptic peptides were analyzed by a high-resolution Q-Exactive HFTM mass spectrometer, and cross-linked peptides were identified by their parent ion mass as well as their subsequent HCD fragment spectra (Figure 7–figure supplement 1). All but one of the five identified cross-links was established between LPL and GPIHBP1's acidic domain, consistent with the abundance of EDC-reactive carboxyl groups in the acidic domain. The corresponding cross-linking sites on LPL included Lys²⁹⁸ in the catalytic domain and Lys⁴¹⁶, Lys⁴²⁴, and Lys⁴³⁰ in the CTD of LPL (Figure 7B). The one cross-linked peptide identified outside of the acidic domain occurred between residues 100–125 (most likely Glu¹⁰²) in the LU-domain of GPIHBP1 and residues 423–430 of LPL. We did not detect cross-links between GPIHBP1³⁴⁻¹³¹ and LPL using 10 mM EDC for 90 min (Figure 7, lanes 6 & 10); however, we did observe such cross-links (Figure 7–figure supplement 2) if we drove the conjugation chemistry to higher yields by converting the *o*-acylisourea EDC intermediate to a more stable amine-reactive derivative (NHS-ester).

DISCUSSION

The interaction between LPL and GPIHBP1 is essential for lipolysis of TRLs along the capillary lumen (Beigneux et al., 2007; Davies et al., 2010; Goulbourne et al., 2014). In the absence of functional GPIHBP1, LPL is mislocalized within the interstitial spaces, leading to severe hypertriglyceridemia and reduced delivery of lipid nutrients to parenchymal cells (Goulbourne et al., 2014; Young and Zechner, 2013). *LPL* or *GPIHBP1* mutations that prevent LPL•GPIHBP1 binding

or abolish LPL catalytic activity result in familial chylomicronemia in humans (Buonuomo et al., 2015; Gin et al., 2012; Henderson et al., 1996; Plengpanich et al., 2014; Rios et al., 2012; Voss et al., 2011). While the physiologic function of GPIHBP1 has gradually come into focus, our understanding of LPL•GPIHBP1 interactions was negligible. No three-dimensional structures had been determined for LPL or GPIHBP1, almost certainly because of the low stability of LPL and earlier difficulties in preparing pure recombinant GPIHBP1 free of protein dimers and multimers (Beigneux et al., 2015).

In the current study, we eliminated one of the roadblocks to progress by developing protocols for expressing and purifying human GPIHBP1. Our approach took advantage of *Drosophila* S2 cells as host cells for heterologous expression. Other LU domain-containing proteins have been expressed with this system (Gårdsvoll et al., 2007; Gårdsvoll et al., 2004), and the high quality of those protein preparations are highlighted by both the structures solved by X-ray crystallography (Lin et al., 2010; Llinas et al., 2005; Xu et al., 2012; Zhao et al., 2015) and the structure–function insights gained by biophysical approaches (HDX-MS, SAXS, and SPR) (Gårdsvoll et al., 2006; Jørgensen et al., 2004; Mertens et al., 2012). In the case of human GPIHBP1, we were able to prepare large quantities of highly purified, monomeric proteins for full-length GPIHBP1^{1–131} as well as a truncated GPIHBP1 lacking the acidic domain (GPIHBP1^{34–131}). The latter protein was generated by limited proteolysis of full-length GPIHBP1.

With the availability of homogeneous preparations of catalytically active LPL and pure, monomeric GPIHBP1, we uncovered several novel properties of the GPIHBP1•LPL interaction, all relevant to the physiology of intravascular TRL processing. We found: [1] that the N-terminal acidic domain of GPIHBP1 is intrinsically disordered; [2] that the acidic domain has a major effect on the association rate constant for the GPIHBP1•LPL interaction; [3] that the time-dependent decay of LPL activity is associated with a global unfolding of LPL's catalytic domain; [4] that the acidic domain of GPIHBP1 preserves the catalytic activity of LPL by mitigating global unfolding of the catalytic domain; and [5] that two discrete interaction sites in the LPL•GPIHBP1 complex cooperate to promote ligand binding and stabilization of LPL catalytic activity.

Our findings have allowed us to conceptualize a model for unoccupied GPIHBP1 in which the N-terminal acidic domain is intrinsically disordered and the remainder of the protein (*i.e.*, GPIHBP1^{34–131}) adopts the prototypical three-finger-fold characteristic of LU domain proteins (Figure 1A). This model was initially suggested by the observation that full-length GPIHBP1 (GPIHBP1^{1–131}) exhibits an unexpectedly large hydrodynamic volume [as judged by its elution profile in size-exclusion chromatography (Figure 1C)], whereas a truncated GPIHBP1 lacking the acidic domain (GPIHBP1^{34–131}) elutes at the expected position for a folded globular protein. The atypical elution profile for the full-length GPIHBP1 is indicative of a large Stokes radius and is one of the hallmarks of intrinsically disordered proteins (Uversky, 2012). Further evidence for the disordered nature of the acidic domain is provided by its highly dynamic state as measured by HDX-MS. Our model offers potential insights into the interplay between GPIHBP1 and LPL during LPL mobilization and TRL processing *in vivo*. In GPIHBP1-deficient mice, the LPL in tissues is mislocalized to the interstitial spaces and never reaches the luminal surface of capillary endothelial cells. It is noteworthy that the LPL in GPIHBP1-deficient mice remains sequestered in the interstitial space, presumably bound to negatively-charged heparin sulfate proteoglycans (HSPGs) (Davies et al., 2010). This interaction is thought to be driven by electrostatic interactions and is characterized by fast kinetic rate constants (Lookene et al., 1996), presumably creating a dynamic reservoir of LPL within the interstitial spaces. In wild-type mice, newly secreted LPL likely binds to the same HSPGs but then moves to GPIHBP1 on capillary endothelial cells. We propose that the intrinsically disordered and markedly acidic N-terminal extension of GPIHBP1 plays an important role in mobilizing HSPG-bound LPL within the interstitial spaces through long-ranged electrostatic interactions, thereby driving LPL into association with endothelial cells. This model for LPL mobilization by GPIHBP1 is consistent with the kinetic rate constants that we determined for GPIHBP1•LPL interactions, which are 10-fold faster for intact GPIHBP1^{1–131} than for GPIHBP1^{34–131} lacking the acidic domain.

Since the difference in k_{on} for GPIHBP1^{1–131} and GPIHBP1^{34–131} is observed for both intact LPL and LPL's CTD alone, we propose that an electrostatic “encounter complex” is initially established

between GPIHBP1's acidic domain and the basic residues in LPL's CTD. This encounter complex then guides the maturation of the interaction, facilitating a tighter binding interface between GPIHBP1's LU domain and residues 402–419 in LPL (Figure 2). The cross-linking that we documented between residues 1–33 of intact GPIHBP1^{1–131} and Lys⁴¹⁶, Lys⁴²⁴, and Lys⁴³⁰ in the CTD of LPL is consistent with this initial encounter/maturation model. The electrostatic component of this model is in accordance with a previous study (Reimund et al., 2015).

The existence of a dual binding mechanism is also consistent with the available mutagenesis data. First, the importance of the positively charged heparin-binding sequences in LPL's CTD has been demonstrated by reduced binding of hLPL^{K403A;R405A;K407A;K413A;K414A} to GPIHBP1 (Gin et al., 2008). Second, there is ample evidence for the involvement of additional CTD sequences—apart from positively charged residues—in the binding of LPL to the LU-domain in GPIHBP1. For example, two missense mutations in LPL (C418Y and E421K), first identified in patients with chylomicronemia, have no effect on heparin binding but abolish binding to GPIHBP1 (Henderson et al., 1998; Henderson et al., 1996; Voss et al., 2011). Lending support to this two-step binding mechanism is the fact that the acidic domain plays little or no role in the stability of established GPIHBP1•LPL complexes. The k_{off} values for GPIHBP1^{1–131} and GPIHBP1^{34–131} are comparable, regardless of whether the binding is to LPL's CTD ($k_{off} = 0.1 \text{ s}^{-1}$) or to full-length LPL ($k_{off} = 0.02 \text{ s}^{-1}$).

A different two-site interaction model between GPIHBP1 and LPL was recently proposed (Reimund et al., 2015), which suggested that a single molecule of GPIHBP1 binds two LPL homodimers. This conclusion was based on SPR studies in which GPIHBP1 (from the medium of transfected CHO cells) had been captured onto chips coated with the anti-GPIHBP1-specific mAb 11A12. To obtain reliable fits for the LPL-binding profiles recorded by SPR and to reduce nonspecific binding of LPL, these authors performed their analyses at 4°C and in the presence of 0.4–0.6 M NaCl. In the current study, the SPR data were obtained under more physiologic conditions (20°C in 0.15 M NaCl), and the binding profiles fit well to a simple 1:1 interaction model (*i.e.*,

GPIHBP1 + LPL₂ \rightleftharpoons GPIHBP1•LPL₂). A likely explanation for the discrepancy between the two studies is the different designs of the SPR studies. The current study measured the binding of purified, monomeric GPIHBP1 in solution to purified LPL that had been captured by mAb 5D2 thereby avoiding the inherent difficulties in having LPL as a soluble analyte. The earlier study measured the interaction between LPL in solution to mouse GPIHBP1 (from the medium of transfected CHO cells) that had been captured on mAb 11A12. We now know the GPIHBP1 secreted from transfected CHO-cells contains significant amounts of dimers and multimers (Beigneux et al., 2015), a factor that would further complicate the interpretation of these SPR data.

An intriguing finding in the current study was the observation that LPL undergoes a time-dependent global unfolding of its catalytic N-terminal domain, as judged by the loss of stable secondary structure in HDX-MS studies (Figure 7). This transition into a pre-molten globule-like conformation of LPL's catalytic domain provides a plausible structural explanation for the time-dependent decline in LPL catalytic activity at room temperature (Osborne et al., 1985). It is noteworthy, however, that unfolding of the catalytic domain in LPL proceeds with only one-half the rate of the parallel loss of catalytic activity. That observation is consistent with a model where the unfolding of one LPL molecule in the homodimer would lead to the inactivation of both subunits.

From our HDX-MS analyses of GPIHBP1•LPL complexes (Figure 2), it is apparent that only one region in LPL responds to the presence of the acidic domain GPIHBP1¹⁻³³, and that is located at the interface between the CTD and the catalytic domain (represented by the peptide spanning residues 279-290) (Figure 7B). The involvement of this “interdomain interface” of LPL in binding GPIHBP1¹⁻³³ was bolstered by zero-length cross-linking studies. The interaction between LPL Lys²⁹⁸ (in close spatial proximity to peptide 279-290) and GPIHBP1's acidic domain was covalently trapped by EDC (Figure 7B). The fact that the acidic domain interacts with the domain interface of LPL in the setting of a mature GPIHBP1•LPL complex likely carries functional implications. Indeed, the stabilization of the catalytic domain of LPL by GPIHBP1¹⁻¹³¹ was primarily mediated by GPIHBP1¹⁻³³ (Table 1). We suspect that the stabilization of LPL's “interdomain interface” by

GPIHBP1's acidic domain serves to limit protein dissociation/unfolding of the partner monomers of an LPL homodimer. Genetic evidence provides circumstantial support for the importance of a properly assembled interdomain interface for LPL activity. Certain homozygous missense mutations that are associated with reduced LPL activity and chylomicronemia [LPL^{E410V}, LPL^{G409R}, and LPL^{S259R} in humans; LPL^{G412R} in cats) (Foubert et al., 1997; Ginzinger et al., 1996; Kassner et al., 2015; Previato et al., 1994)] are located at the interdomain interface in close spatial proximity to the proposed binding site in LPL^{279–290} for GPIHBP1^{1–33} (Figure 7B). All mutations alter the electrostatics of the interface. In future studies, it will also be very interesting to investigate if the accelerated inactivation of LPL by ANGPTL4 (Sukonina et al., 2006) involves this interdomain region and the extent to which GPIHBP1 protects LPL from ANGPTL4-mediated inactivation.

From a practical point of view, our discovery that the acidic domain stabilizes the conformation of LPL by mitigating unfolding could prove to be helpful in future efforts to define the structure of LPL by X-ray crystallography. We suspect that incubating LPL with peptides derived from GPIHBP1's acidic domain could promote stabilization of LPL, increase its conformational homogeneity, and enhance the likelihood of growing well-diffracting crystals for X-ray structure determination.

Materials and Methods

Purified proteins and reagents

Bovine LPL was purified from fresh bovine milk by heparin-Sepharose, hydroxyapatite, and Superdex HR200 size-exclusion chromatography as described (Cheng et al., 1985). Fractions containing dimeric LPL (LPL₂) were precipitated with 3.6 M NH₄SO₄ and the pellet dissolved in 5 mM phosphate buffer (pH 6.5) containing 40% (v/v) glycerol. Small aliquots were stored at –80°C until use. Recombinant enterokinase (1 U/μl) produced in *Pichia pastoris* (EKMax™) was purchased from Invitrogen (Carlsbad, CA). Monoclonal antibodies against human uPAR (R2 and R24) and human LPL (5D2 and 4-1A) were produced and characterized as described (Bensadoun et al., 2014; Chang et al., 1998; Gårdsvoll et al., 2011). A synthetic 33-mer peptide (GPIHBP1^{1–33}) representing the N-terminal acidic domain of GPIHBP1 (QTQQEEEEDEDHGPDDYDEEEDEVVEEETNR) was obtained at a purity of >95% from TAG-Copenhagen A/S (Copenhagen, Denmark).

Expression and purification of human GPIHBP1 and LPL^{313–348} by *Drosophila* S2-cells

A truncated version of human GPIHBP1 (residues 1–131), lacking the C-terminal signal peptide that normally triggers the covalent addition of a glycolipid-anchor, was expressed by (and secreted from) *Drosophila* S2 cells as a fusion protein with uPAR domain III (RS-DIII-ent-GPIHBP1, Figure 1–figure supplement 1A). This strategy has been used for expressing other LU-domain proteins (Gårdsvoll et al., 2007; Gårdsvoll et al., 2013; Hansen et al., 2004). The N-terminal uPAR DIII serves dual roles as detection and purification tag, and the DDDDK motif in the linker region allows excision of GPIHBP1 by enterokinase cleavage while preserving the original N-terminus of GPIHBP1. Using this strategy, we also expressed the mutants RS-DIII-ent-GPIHBP1^{W89S} and RS-DIII^{R281G}-ent-GPIHBP1^{R38G}. The latter construct was designed to improve the overall yield of

purified intact GPIHBP1 after enterokinase cleavage.

A similar platform was employed to express the C-terminal domain (CTD) of human LPL (residues 313–448) using constructs RS-DIII-ent-CTD and RS-DIII-ent-CTD^{C418Y} (Figure 1–figure supplement 1B).

After 7 days of induction with 0.5 mM CuSO₄, the medium from the *Drosophila* S2 cells was harvested and supplemented with 0.1 volume of 1 M Tris/HCl (pH 8.0) containing 0.2 M EDTA and 0.1% (w/v) NaN₃ and 0.005 volume of 200 mM PMSF in DMSO. The various RS-DIII-ent-GPIHBP1 proteins were purified from the medium of transfected cells by immunoaffinity chromatography with an anti-uPAR mAb R2 column with 0.1 M CH₃COOH, 0.5 M NaCl (pH 2.5) as the eluent. The purified proteins were exchanged into 20 mM NaH₂PO₄, 150 mM NaCl (pH 7.2) and stored at –80°C. The RS-DIII-ent-CTD constructs were affinity purified with an anti-uPAR mAb R24 column (Gårdsvoll et al., 2011) and eluted with 0.1 M CH₃COOH, 0.5 M NaCl (pH 2.5) containing 20% (v/v) glycerol and then exchanged into 20 mM NaH₂PO₄, 150 mM NaCl (pH 7.2) containing 20% (v/v) glycerol to prevent precipitation. Average yields of the fusion proteins were 2–5 mg per liter.

Enterokinase cleavage and purification of human GPIHBP1

The DIII-tag was removed from the purified fusion proteins by adding 0.1 U enterokinase/mg and incubating at 37°C. An equal amount of enterokinase was added 6 h later, and the incubation was continued for a total of 24 h. This digest was dialyzed against 50 mM CH₃COOH (pH 4.5). The excised GPIHBP1 was purified by cation-exchange chromatography with a 5-ml HiTrap SP FF™ (GE Healthcare; Uppsala, Sweden) and a 35-ml linear NaCl gradient (from 0 to 1.0 M) in 50 mM CH₃COOH (pH 4.5) (Figure 1–figure supplement 2A). Relevant fractions were pooled and buffer-

exchanged into 20 mM NaH_2PO_4 , 150 mM NaCl (pH 7.2) before conducting a final purification step by size-exclusion chromatography on a Superdex HR75 column in the same buffer (Figure 1C).

Affinity of the GPIHBP1•LPL interaction as assessed by surface plasmon resonance

To minimize confounding effects resulting from the dextran surface of the sensor chip on the real-time kinetics recorded for the LPL•GPIHBP1 interaction, we used a CM4 sensor chip with a low degree of carboxylation to immobilize the LPL-specific monoclonal antibody 5D2 (Chang et al., 1998). As a further precaution, we used 1 M ethylenediamine rather than ethanolamine to block excess active N-hydroxysuccinimide esters (NHS), which reduces the charge effects from the remaining unmodified carboxylates on the matrix (Glaser et al., 2014). Covalent immobilization of mAb 5D2 was accomplished by injecting 5 $\mu\text{g}/\text{ml}$ 5D2 dissolved in 10 mM sodium acetate (pH 5.0) over a CM4 chip that had been pre-activated with NHS/EDC (N-ethyl-N'-[3-diethylamino)propyl]-carbodiimide), aiming at a surface density of 1500 resonance units (RU) corresponding to 10 fmols/ mm^2 .

After a 100-sec loading pulse with 100 nM recombinant LPL CTD^{313–448} at 20 $\mu\text{l}/\text{min}$, real-time interactions between 5D2-captured CTDs (~ 100 –200 RU; 6–12 fmol/ mm^2) and serial twofold dilutions of purified human GPIHBP1 were measured from 8 nM to 4 μM at 20°C using 10 mM HEPES, 150 mM NaCl, 3 mM EDTA (pH 7.4) containing 0.05% (v/v) surfactant P20 as running buffer. To be confident of a high reproducibility, at least one GPIHBP1 concentration was re-tested at the end of each experiment. Between cycles, mAb 5D2 was regenerated with two consecutive 10- μl injections of 0.1 M acetic acid/HCl (pH 2.5) in 0.5 M NaCl and 20 mM H_3PO_4 . The immobilized mAb 5D2 tolerated repetitive regenerations without significant decline of its capturing capacity.

After double-buffer referencing of the recorded real-time interaction analyses, the kinetic rate constants (k_{on} and k_{off}) were derived by global non-linear regression fitting of the association and dissociation phases to a simple bimolecular interaction model, including correction for mass transport limitations assuming pseudo-first-order reaction conditions with BIAevaluation 4.1 software

(Biacore, Uppsala, Sweden). In some cases, the equilibrium binding constants K_D and R_{\max} were also calculated separately from the corresponding equilibrium binding isotherms by nonlinear curve fitting assuming saturation of a single binding site:

$$R_{\text{eq}} = (R_{\max}[\text{GPIHBP1}]) / (K_d + [\text{GPIHBP1}]),$$

where R_{eq} is the binding level at equilibrium, and R_{\max} is the binding capacity of the chip.

To enable efficient capturing of intact dimeric bovine LPL (LPL_2) on immobilized mAb 5D2, the purified LPL_2 was diluted 500–1000 fold to 200 nM in 10 mM HEPES (pH 7.4), 150 mM NaCl, 4 mM CaCl_2 , 0.05% (v/v) surfactant P20 supplemented with 0.2 mg/ml BSA and 1% (w/v) carboxymethyl dextran to stabilize LPL and avoid non-specific adsorption to the microfluidics during loading. The running buffer was equivalent to the loading buffer except that no carboxymethyl dextran was added. Regeneration of the capturing mAb was accomplished by two consecutive injections of 10 μl of 20 mM glycine/HCl (pH 2.5) and 10 μl of 5% (v/v) HCOOH -containing 0.5 M NaCl. To minimize deterioration from repetitive regenerations, single-cycle kinetic titration (Karlsson et al., 2006) of $\text{LPL} \cdot \text{GPIHBP1}$ interactions were recorded during five consecutive injections of 20 μl of twofold dilutions of purified GPIHBP1 at 20°C. After double-buffer referencing of the data, the corresponding kinetic rate constants were derived by fitting the data to a simple bimolecular interaction model using the mathematic model developed for single-cycle kinetics (T200 Evaluation Software 2.0, GE Healthcare Life Science, Uppsala, Sweden).

Equilibrium binding constants of the GPIHBP1•LPL interaction by microscale thermophoresis

To determine solution equilibrium binding constants between LPL and Alexa Flour-647–labeled versions of $\text{GPIHBP1}^{1-131/\text{R38G}}$ and $\text{GPIHBP1}^{34-131/\text{R38G}}$, we used microscale thermophoresis technology (Jerabek-Willemsen et al., 2014). Purified $\text{GPIHBP1}^{1-131/\text{R38G}}$ and $\text{GPIHBP1}^{34-131/\text{R38G}}$

preparations were labeled for 30 min at 37°C with Alexa Flour-647 NHS ester (Thermo Fisher Scientific) at a molar ratio of 1:3 in PBS (pH 7.4); these conditions modification of the N-terminal α -amino group. The reaction was terminated by adding 10 mM ethanolamine, and the proteins were desalted on a PD-10 column (GE Healthcare, Uppsala, Sweden). The average degree of labeling was 1.3 fluorephore/protein for both GPIHBP1^{1-131/R38G} and GPIHBP1^{34-131/R38G}; both labeled proteins remained monomeric as judged by analytical size-exclusion chromatography on a 5/150 SuperdexTM75 column (GE Healthcare, Uppsala, Sweden). The equilibrium binding between 5 nM Alexa Flour-647-labeled GPIHBP1 and LPL were calculated from the change in thermophoresis ($\Delta F_{\text{norm}} = F_{\text{Hot}}/F_{\text{cold}}$) measured with a Monolith NT.115 (NanoTemper Technologies GmbH) after adding increasing concentrations of non-fluorescent LPL. A two-fold dilution series ranging from 10 pM to 350 nM LPL₂ was prepared in 10 mM HEPES (pH 7.4), 150 mM NaCl, 4 mM CaCl₂, 0.05% (v/v) surfactant P20, and 1.0 mg/ml BSA. Samples were loaded into low-binding hydrophilic capillary tubes and the thermophoresis signals were measured at 22°C with a LED power of 80% and an IR laser power of 100%.

Determination of lipase and esterase activity of purified LPL

Time-dependent inactivation profiles for LPL were determined by incubating 2 μ M purified LPL₂ alone or in the presence of 2 μ M GPIHBP1¹⁻¹³¹, 2 μ M GPIHBP1³⁴⁻¹³¹, or 10 μ M GPIHBP1¹⁻³³ for various times at 25°C in 10 mM Na₂HPO₄, 150 mM NaCl (pH 7.4). The temperature-induced unfolding was quenched by adding ice-cold 100 mM Tris (pH 7.8) containing 5 mM deoxycholic acid (DOC) and 0.1 mM sodium dodecyl sulfate (SDS) (DOC/SDS buffer). Esterase activities were analyzed by mixing 5 μ l of LPL diluted 100-fold in DOC/SDS buffer with 95 μ l DGGR assay buffer to a final concentration of 50 mM Tris, 50 μ M 1,2-o-dilauryl-rac-glycero glutaric acid-(6'-methylresorufin) ester (DGGR), 120 mM NaCl, 10 mg/ml BSA, 0.5% Triton X-100 (v/v), pH 7.4. Ester hydrolysis was determined by measuring the linear increase of resorufin fluorescence

at λ_{ex} 530 nm, λ_{em} 590 nm during the initial 5 min. Lipase activities were determined by adding 5 μl of LPL diluted 1000-fold in DOC/SDS to 195 μl of incubation mixtures with Intralipid containing [^3H]triolein (Larsson et al., 2013).

Protein dynamics measured by HDX-MS

All hydrogen–deuterium exchange reactions were performed at 25°C and 300 RPM mixing, using 10 mM Na_2HPO_4 , 150 mM NaCl buffers in either H_2O or D_2O , adjusted to pH 7.4 and pD 7.4 ($\text{pH}_{\text{read}} = 7.0$), respectively. The following protein solutions were made with the H_2O buffer: 5 μM LPL₂, 5 μM GPIHBP1^{1–131/R38G}, 5 μM LPL₂ + 5 μM GPIHBP1^{1–131/R38G}, 5 μM LPL₂ + 25 μM GPIHBP1^{1–33}. Most solutions were pre-incubated for 15 min before deuterium labeling to promote efficient complex formation. Samples containing exclusively LPL₂ were not pre-incubated because of concerns about the inherent instability of LPL homodimers.

Isotopic labeling was initiated by adding D_2O buffer to the protein solutions to a final concentration of 70% D_2O (vol/vol). After 10-, 100- or 1,000-sec, aliquots were collected from the labeling solutions. These were mixed with 1 volume ice-cold quenching buffer (100 mM Na_2HPO_4 , 0.8 M TCEP, 2 M urea in H_2O , pH 2.5). Quenched samples were placed in an ice bath for 2 min to reduce disulfide bonds and subsequently snap-frozen in liquid nitrogen.

Full deuteration controls were prepared by (1) diluting LPL and GPIHBP1 to 10 μM in 10 mM Na_2HPO_4 , 150 mM NaCl, 2 M urea, 70% (vol/vol) D_2O , pD 7.4; (2) incubating samples for 48 h at 37°C; and (3) quenching as described above without urea to achieve an identical solvent composition in the quenched samples. Labeling was performed in triplicate for each sample combination.

Unfolding of LPL assessed by pulse-labeling HDX-MS

Buffers and labeling conditions were identical to those described previously. The following protein solutions were prepared in H_2O buffer: 5 μM LPL₂, 5 μM LPL₂ + 5 μM GPIHBP1^{1–131/R38G}, 5 μM

LPL₂ + 5 μ M GPIHBP1^{1–33}, and 5 μ M LPL₂ + 5 μ M GPIHBP1^{34–131/R38G}. Solutions were incubated for 15, 30, 45, 60, 90, and 120 min, diluted to 70% D₂O buffer, allowed to exchange for 10 sec, quenched by adding 1:1 ice-cold quench buffer, incubated for 2 min in an ice bath, and then snap frozen. Labeling was performed in triplicate for each sample combination incubated at 45 min.

MS of HDX-labeled samples and data analysis

Quenched and reduced samples were analyzed with a nanoACQUITY UPLC reversed-phased chromatographic system equipped with HDX technology (Waters, Milford, MA) coupled to a Synapt G2 electrospray ionization mass spectrometer (Waters). Desalting was performed by applying a flow of 300 μ L/min buffer A [0.23% (v/v) formic acid (FA)] to an ACQUITY UPLC BEH C18 1.7- μ m, 2.1 \times 5 mm Vanguard Pre-Column by an Agilent 1260 Infinity Quaternary pump (Agilent Technologies, Santa Clara, CA). Peptides were separated on a 1.0 \times 100 mm ACQUITY UPLC BEH C18 1.7- μ m analytical column by a 12-min gradient from 95% buffer A to 50% buffer B [0.23% (v/v) FA in acetonitrile] at a flow of 40 μ L/min. Proteins were digested online with an Upchurch guard column (1.0 \times 20 mm, IDEX, Oak Harbor, WA, USA) packed with agarose-immobilized pepsin (Thermo Scientific Pierce, Rockford, IL). Peptides from peptic digests were identified from DDA MS/MS runs using ProteinLynx Global Server v2.4 (Waters) and MassAI v1.07 (MassAI Bioinformatics, Stenstrup, DK, <http://www.massai.dk>). Deuterium incorporation for intact proteins and peptides was quantified with DynamX V2.0 (Waters).

Homology modeling and disorder prediction for GPIHBP1

Human GPIHBP1 (UniProt id: Q8VI16) without the N- and C-terminal signal sequences was used for a homology search with the program HHPred (Soding, 2005). To find suitable reference structures,

the PDB database was used to generate a multiple sequence alignment with human GPIHBP1; the top five highest-ranking proteins (PDB entries: 20l3, 2h7z, 2h5f, 3neq, 1hcp) were selected as templates for homology modeling with MODELLER (Sali et al., 1995). Molecular structures are displayed by PyMOL (Schrödinger, LLC). A search for regions in human GPIHBP1 with a high propensity for intrinsic disorder was performed with the disorder prediction tools IUPred (Dosztanyi et al., 2005) and DISOPRED3 (Jones and Cozzetto, 2015).

Zero-length chemical cross-linking of GPIHBP1•LPL complexes

To initiate covalent cross-linking, mixtures of 1.5 μM LPL₂ with either 7 μM GPIHBP1^{1–131}, 7 μM GPIHBP1^{34–131}, or 15 μM GPIHBP1^{1–33} were exposed to 10 mM EDC for 90 min at 25°C in 10 mM Na₂HPO₄ (pH 8.0), 150 mM NaCl, 0.1% (v/v) Triton X-100, and 10% (v/v) glycerol. The cross-linking reaction was terminated by boiling in SDS-PAGE sample buffer; samples were subsequently reduced and alkylated before analysis by SDS-PAGE to assess the formation of covalent complexes. Cross-linked tryptic peptides were identified by high-resolution mass spectrometry with a Q-Exactive HF mass spectrometer (Thermo Scientific).

In-gel digestion and desalting of cross-linked LPL•GPIHBP1^{1–131} complexes

Coomassie Blue–stained protein bands corresponding to cross-linked protein complexes were excised from the polyacrylamide gel and subjected to in-gel reduction, alkylation and digestion with trypsin, as described with minor modifications (Shevchenko et al., 1996). Gel pieces were cut into smaller pieces, washed twice in 50% ethanol (v/v) and shrunk with 96% (v/v) ethanol. The shrunken gel pieces were then swollen in a 10 mM dithiothreitol (DTT) 0.1 M NH₄HCO₃ solution and incubated for 45 min at 56°C. After reduction, the solution was cooled to room temperature. The excess DTT

solution was removed and replaced with a 55 mM iodoacetamide (IAA) 0.1 M NH_4HCO_3 solution followed by incubation for 30 min in the dark at room temperature. Excess IAA solution was removed; the gel pieces were washed twice in 50% ethanol (v/v) and the gel pieces were shrunk again using 96% (v/v) ethanol. Finally, the gel pieces were rehydrated on ice with a 100 mM NH_4HCO_3 solution containing 12.5 ng/ μl trypsin. After 45 min, excess trypsin solution was removed and replaced with 100 mM NH_4HCO_3 , and the gel pieces were then incubated at 37°C overnight. The supernatant containing tryptic peptides was recovered the next day. Remaining peptides in the gel were extracted by adding 5% (v/v) formic acid, incubating for 15 min, and then adding an equal volume of acetonitrile and incubating for an additional 15 min. This supernatant was combined with the original supernatant and the entire pool dried in a vacuum centrifuge. Prior to analysis, the tryptic digest was resuspended in 0.1% trifluoroacetic acid (TFA) and desalted using solid-phase extraction in a pipet tip packed with Oligo R3 reversed phase resin (Applied Biosystems). The column was subsequently washed with 0.1% (v/v) TFA; the bound sample was eluted with 0.1% (v/v) TFA in 70% (v/v) acetonitrile and then dried in a vacuum centrifuge.

Reversed-phase nano-LC-ESI-MS/MS

The samples were resuspended in 0.1% (v/v) FA and loaded onto an EASY-nLC system (Thermo Scientific) with a two-column setup. Trapping was performed with a 100 $\mu\text{m} \times 2$ cm Acclaim PepMap100 C18 Nano-Trap Column and peptides were separated along a 75 $\mu\text{m} \times 25$ cm Acclaim PepMap RSLC analytical column (both Thermo Scientific). The peptides were eluted with an organic solvent gradient from 95% phase A [0.1% (v/v) FA] to 25% phase B [0.1% (v/v) FA, 95% (v/v) acetonitrile] over 80 min, followed by a 10-min gradient to 50% phase B at a flow rate of 250 nl/min. The eluted peptides were analyzed with a Q-Exactive HF mass spectrometer (Thermo Scientific), operated in the positive ionization mode with data-dependent acquisition. Each MS scan was acquired

at a resolution of 60,000 FWHM followed by 20 high-resolution HCD-MS/MS scans of the most intense ions. Ions selected for MS/MS were dynamically excluded for durations of 10 sec.

Data analysis

MGF files were generated from the raw data with Proteome Discoverer v1.3 (Thermo Scientific), and the protein crosslinks identified using MassAI (Peng et al., 2014) (www.MassAI.dk). Searches against a database containing bovine LPL and GPIHBP1 R38G were performed with the following parameters: Precursor mass tolerance 10 ppm, MS/MS mass tolerance of 0.05 Da, tryptic cleavage allowing up to two missed cleavage sites, and carbamido-methylation of cysteine as a fixed modification. The following variable modifications were allowed: oxidation of Met; phosphorylation of Ser, Thr, and Tyr; and N-glycosylation of Asn-X-Ser/Thr/Cys. Peptide cross-links between Lys and Asp/Glu, with a resulting loss of water, were allowed. Cross-links were considered to be true if they had a score above 20 and the MS/MS spectra either contained fragment ion series originating from both peptides, or contained peaks that represented cross-linked fragment ions.

Acknowledgments

The coordinates for the model of human LPL were provided by Dr. Z. Liu (School of Pharmaceutical Sciences, Beijing, China). We acknowledge Gry Rasmussen, Haldis Egholm, and Gitte Juhl Funch for expert technical assistance and John Post for artwork. This work was supported by a Leducq Transatlantic Network grant (12CVD04) and by NIH grants HL090553 and HL087228. The authors have no financial interests to declare.

References

- Beigneux, A.P., Davies, B.S., Gin, P., Weinstein, M.M., Farber, E., Qiao, X., Peale, F., *et al.* (2007). Glycosylphosphatidylinositol-anchored high-density lipoprotein-binding protein 1 plays a critical role in the lipolytic processing of chylomicrons. *Cell Metab* 5, 279-291.
- Beigneux, A.P., Davies, B.S., Tat, S., Chen, J., Gin, P., Voss, C.V., Weinstein, M.M., *et al.* (2011). Assessing the role of the glycosylphosphatidylinositol-anchored high density lipoprotein-binding protein 1 (GPIHBP1) three-finger domain in binding lipoprotein lipase. *J Biol Chem* 286, 19735-19743.
- Beigneux, A.P., Fong, L.G., Bensadoun, A., Davies, B.S., Oberer, M., Gårdsvoll, H., Ploug, M., *et al.* (2015). GPIHBP1 Missense Mutations Often Cause Multimerization of GPIHBP1 and Thereby Prevent Lipoprotein Lipase Binding. *Circ Res* 116, 624-632.
- Beigneux, A.P., Franssen, R., Bensadoun, A., Gin, P., Melford, K., Peter, J., Walzem, R.L., *et al.* (2009). Chylomicronemia With a Mutant GPIHBP1 (Q115P) That Cannot Bind Lipoprotein Lipase. *Arteriosclerosis Thrombosis and Vascular Biology* 29, 956-U447.
- Bensadoun, A., Mottler, C.D., Pelletier, C., Wu, D., Seo, J.J., Leung, C.S., Adeyo, O., *et al.* (2014). A new monoclonal antibody, 4-1a, that binds to the amino terminus of human lipoprotein lipase. *Biochim Biophys Acta* 1841, 970-976.
- Brahm, A.J., and Hegele, R.A. (2015). Chylomicronaemia-current diagnosis and future therapies. *Nat Rev Endocrinol* 11, 352-362.
- Brown, W.V., Goldberg, I.J., and Young, S.G. (2015). JCL Roundtable: Hypertriglyceridemia due to defects in lipoprotein lipase function. *J Clin Lipidol* 9, 274-280.
- Buonuomo, P.S., Bartuli, A., Rabacchi, C., Bertolini, S., and Calandra, S. (2015). A 3-day-old neonate with severe hypertriglyceridemia from novel mutations of the GPIHBP1 gene. *J Clin Lipidol* 9, 265-270.
- Chang, S.F., Reich, B., Brunzell, J.D., and Will, H. (1998). Detailed characterization of the binding site of the lipoprotein lipase-specific monoclonal antibody 5D2. *J Lipid Res* 39, 2350-2359.
- Cheng, C.F., Bensadoun, A., Bersot, T., Hsu, J.S., and Melford, K.H. (1985). Purification and characterization of human lipoprotein lipase and hepatic triglyceride lipase. Reactivity with monoclonal antibodies to hepatic triglyceride lipase. *J Biol Chem* 260, 10720-10727.
- Davies, B.S., Beigneux, A.P., Barnes, R.H., 2nd, Tu, Y., Gin, P., Weinstein, M.M., Nobumori, C., *et al.* (2010). GPIHBP1 is responsible for the entry of lipoprotein lipase into capillaries. *Cell Metab* 12, 42-52.
- Dosztanyi, Z., Csizmok, V., Tompa, P., and Simon, I. (2005). IUPred: web server for the prediction of intrinsically unstructured regions of proteins based on estimated energy content. *Bioinformatics* 21, 3433-3434.

- Foubert, L., Bruin, T., De Gennes, J.L., Ehrenborg, E., Furioli, J., Kastelein, J., Benlian, P., *et al.* (1997). A single Ser259Arg mutation in the gene for lipoprotein lipase causes chylomicronemia in Moroccans of Berber ancestry. *Hum Mutat* 10, 179-185.
- Gin, P., Goulbourne, C.N., Adeyo, O., Beigneux, A.P., Davies, B.S., Tat, S., Voss, C.V., *et al.* (2012). Chylomicronemia mutations yield new insights into interactions between lipoprotein lipase and GPIHBP1. *Hum Mol Genet* 21, 2961-2972.
- Gin, P., Yin, L., Davies, B.S., Weinstein, M.M., Ryan, R.O., Bensadoun, A., Fong, L.G., *et al.* (2008). The acidic domain of GPIHBP1 is important for the binding of lipoprotein lipase and chylomicrons. *J Biol Chem* 283, 29554-29562.
- Ginzinger, D.G., Lewis, M.E., Ma, Y., Jones, B.R., Liu, G., and Jones, S.D. (1996). A mutation in the lipoprotein lipase gene is the molecular basis of chylomicronemia in a colony of domestic cats. *J Clin Invest* 97, 1257-1266.
- Glaser, R.W., Schonherr, R., and Heinemann, S.H. (2014). Fixed charges in the gel matrix of sensor chips and dissociation in diffusion gradients influence the detection of fast protein-protein interactions. *Biosystems* 116, 27-35.
- Goulbourne, C.N., Gin, P., Tatar, A., Nobumori, C., Hoenger, A., Jiang, H., Grovenor, C.R., *et al.* (2014). The GPIHBP1-LPL complex is responsible for the margination of triglyceride-rich lipoproteins in capillaries. *Cell Metab* 19, 849-860.
- Gårdsvoll, H., Gilquin, B., Le Du, M.H., Menez, A., Jørgensen, T.J., and Ploug, M. (2006). Characterization of the functional epitope on the urokinase receptor. Complete alanine scanning mutagenesis supplemented by chemical cross-linking. *J Biol Chem* 281, 19260-19272.
- Gårdsvoll, H., Hansen, L.V., Jørgensen, T.J., and Ploug, M. (2007). A new tagging system for production of recombinant proteins in *Drosophila* S2 cells using the third domain of the urokinase receptor. *Protein Expr Purif* 52, 384-394.
- Gårdsvoll, H., Jacobsen, B., Kriegbaum, M.C., Behrendt, N., Engelholm, L., Østergaard, S., and Ploug, M. (2011). Conformational regulation of urokinase receptor function: impact of receptor occupancy and epitope-mapped monoclonal antibodies on lamellipodia induction. *J Biol Chem* 286, 33544-33556.
- Gårdsvoll, H., Kriegbaum, M.C., Hertz, E.P., Alpizar-Alpizar, W., and Ploug, M. (2013). The urokinase receptor homolog Haldisin is a novel differentiation marker of stratum granulosum in squamous epithelia. *J Histochem Cytochem* 61, 802-813.
- Gårdsvoll, H., Werner, F., Søndergaard, L., Danø, K., and Ploug, M. (2004). Characterization of low-glycosylated forms of soluble human urokinase receptor expressed in *Drosophila* Schneider 2 cells after deletion of glycosylation-sites. *Protein Expr Purif* 34, 284-295.
- Hansen, L.V., Gårdsvoll, H., Nielsen, B.S., Lund, L.R., Danø, K., Jensen, O.N., and Ploug, M. (2004). Structural analysis and tissue localization of human C4.4A: a protein homologue of the urokinase receptor. *Biochem J* 380, 845-857.

- Hata, A., Ridinger, D.N., Sutherland, S., Emi, M., Shuhua, Z., Myers, R.L., Ren, K., *et al.* (1993). Binding of lipoprotein lipase to heparin. Identification of five critical residues in two distinct segments of the amino-terminal domain. *J Biol Chem* 268, 8447-8457.
- Henderson, H., Leisegang, F., Hassan, F., Hayden, M., and Marais, D. (1998). A novel Glu421Lys substitution in the lipoprotein lipase gene in pregnancy-induced hypertriglyceridemic pancreatitis. *Clin Chim Acta* 269, 1-12.
- Henderson, H.E., Hassan, F., Marais, D., and Hayden, M.R. (1996). A new mutation destroying disulphide bridging in the C-terminal domain of lipoprotein lipase. *Biochem Biophys Res Commun* 227, 189-194.
- Jerabek-Willemsen, M., André, T., Wanner, R., Roth, H.M., Duhr, S., Baaske, P., and Breitsprecher, D. (2014). MicroScale Thermophoresis: Interaction analysis and beyond. *Journal of Molecular Structure* 1077, 101-113.
- Jones, D.T., and Cozzetto, D. (2015). DISOPRED3: precise disordered region predictions with annotated protein-binding activity. *Bioinformatics* 31, 857-863.
- Jørgensen, T.J., Gårdsvoll, H., Danø, K., Roepstorff, P., and Ploug, M. (2004). Dynamics of urokinase receptor interaction with Peptide antagonists studied by amide hydrogen exchange and mass spectrometry. *Biochemistry* 43, 15044-15057.
- Karlsson, R., Katsamba, P.S., Nordin, H., Pol, E., and Myszk, D.G. (2006). Analyzing a kinetic titration series using affinity biosensors. *Anal Biochem* 349, 136-147.
- Kassner, U., Salewsky, B., Wuhle-Demuth, M., Szijarto, I.A., Grenkowitz, T., Binner, P., Marz, W., *et al.* (2015). Severe hypertriglyceridemia in a patient heterozygous for a lipoprotein lipase gene allele with two novel missense variants. *Eur J Hum Genet*.
- Kobayashi, Y., Nakajima, T., and Inoue, I. (2002). Molecular modeling of the dimeric structure of human lipoprotein lipase and functional studies of the carboxyl-terminal domain. *Eur J Biochem* 269, 4701-4710.
- Korn, E.D. (1955). Clearing factor, a heparin-activated lipoprotein lipase. I. Isolation and characterization of the enzyme from normal rat heart. *J Biol Chem* 215, 1-14.
- Kriegbaum, M.C., Persson, M., Haldager, L., Alpizar-Alpizar, W., Jacobsen, B., Gårdsvoll, H., Kjaer, A., *et al.* (2011). Rational targeting of the urokinase receptor (uPAR): development of antagonists and non-invasive imaging probes. *Curr Drug Targets* 12, 1711-1728.
- Larsson, M., Vorrso, E., Talmud, P., Lookene, A., and Olivecrona, G. (2013). Apolipoproteins C-I and C-III inhibit lipoprotein lipase activity by displacement of the enzyme from lipid droplets. *J Biol Chem* 288, 33997-34008.
- Lin, L., Gårdsvoll, H., Huai, Q., Huang, M., and Ploug, M. (2010). Structure-based engineering of species selectivity in the interaction between urokinase and its receptor: implication for preclinical cancer therapy. *J Biol Chem* 285, 10982-10992.

- Llinas, P., Le Du, M.H., Gårdsvoll, H., Danø, K., Ploug, M., Gilquin, B., Stura, E.A., *et al.* (2005). Crystal structure of the human urokinase plasminogen activator receptor bound to an antagonist peptide. *EMBO J* 24, 1655-1663.
- Lookene, A., Chevreuil, O., Østergård, P., and Olivecrona, G. (1996). Interaction of lipoprotein lipase with heparin fragments and with heparan sulfate: stoichiometry, stabilization, and kinetics. *Biochemistry* 35, 12155-12163.
- Mertens, H.D., Kjaergaard, M., Mysling, S., Gårdsvoll, H., Jørgensen, T.J., Svergun, D.I., and Ploug, M. (2012). A flexible multidomain structure drives the function of the urokinase-type plasminogen activator receptor (uPAR). *J Biol Chem* 287, 34304-34315.
- Olivecrona, G., Ehrenborg, E., Semb, H., Makoveichuk, E., Lindberg, A., Hayden, M.R., Gin, P., *et al.* (2010). Mutation of conserved cysteines in the Ly6 domain of GPIHBP1 in familial chylomicronemia. *Journal of Lipid Research* 51, 1535-1545.
- Osborne, J.C., Jr., Bengtsson-Olivecrona, G., Lee, N.S., and Olivecrona, T. (1985). Studies on inactivation of lipoprotein lipase: role of the dimer to monomer dissociation. *Biochemistry* 24, 5606-5611.
- Peng, L., Rasmussen, M.I., Chailyan, A., Houen, G., and Hojrup, P. (2014). Probing the structure of human protein disulfide isomerase by chemical cross-linking combined with mass spectrometry. *J Proteomics* 108, 1-16.
- Plengpanich, W., Young, S.G., Khovidhunkit, W., Bensadoun, A., Karnman, H., Ploug, M., Gårdsvoll, H., *et al.* (2014). Multimerization of glycosylphosphatidylinositol-anchored high density lipoprotein-binding protein 1 (GPIHBP1) and familial chylomicronemia from a serine-to-cysteine substitution in GPIHBP1 Ly6 domain. *J Biol Chem* 289, 19491-19499.
- Ploug, M. (2003). Structure-function relationships in the interaction between the urokinase-type plasminogen activator and its receptor. *Curr Pharm Des* 9, 1499-1528.
- Previato, L., Guardamagna, O., Dugi, K.A., Ronan, R., Talley, G.D., Santamarina-Fojo, S., and Brewer, H.B., Jr. (1994). A novel missense mutation in the C-terminal domain of lipoprotein lipase (Glu410-->Val) leads to enzyme inactivation and familial chylomicronemia. *J Lipid Res* 35, 1552-1560.
- Reimund, M., Larsson, M., Kovrov, O., Kasvandik, S., Olivecrona, G., and Lookene, A. (2015). Evidence for Two Distinct Binding Sites for Lipoprotein Lipase on Glycosylphosphatidylinositol-anchored High Density Lipoprotein-binding Protein 1 (GPIHBP1). *J Biol Chem*.
- Rios, J.J., Shastry, S., Jasso, J., Hauser, N., Garg, A., Bensadoun, A., Cohen, J.C., *et al.* (2012). Deletion of GPIHBP1 causing severe chylomicronemia. *J Inherit Metab Dis* 35, 531-540.
- Sali, A., Potterton, L., Yuan, F., van Vlijmen, H., and Karplus, M. (1995). Evaluation of comparative protein modeling by MODELLER. *Proteins* 23, 318-326.
- Shevchenko, A., Wilm, M., Vorm, O., and Mann, M. (1996). Mass spectrometric sequencing of proteins silver-stained polyacrylamide gels. *Anal Chem* 68, 850-858.
- Soding, J. (2005). Protein homology detection by HMM-HMM comparison. *Bioinformatics* 21, 951-960.

- Sukonina, V., Lookene, A., Olivecrona, T., and Olivecrona, G. (2006). Angiopoietin-like protein 4 converts lipoprotein lipase to inactive monomers and modulates lipase activity in adipose tissue. *Proc Natl Acad Sci U S A* 103, 17450-17455.
- Surendran, R.P., Visser, M.E., Heemelaar, S., Wang, J., Peter, J., Defesche, J.C., Kuivenhoven, J.A., *et al.* (2012). Mutations in LPL, APOC2, APOA5, GPIHBP1 and LMF1 in patients with severe hypertriglyceridaemia. *J Intern Med* 272, 185-196.
- Uversky, V.N. (2012). Size-exclusion chromatography in structural analysis of intrinsically disordered proteins. *Methods Mol Biol* 896, 179-194.
- Voss, C.V., Davies, B.S., Tat, S., Gin, P., Fong, L.G., Pelletier, C., Mottler, C.D., *et al.* (2011). Mutations in lipoprotein lipase that block binding to the endothelial cell transporter GPIHBP1. *Proc Natl Acad Sci U S A* 108, 7980-7984.
- Xu, X., Gårdsvoll, H., Yuan, C., Lin, L., Ploug, M., and Huang, M. (2012). Crystal structure of the urokinase receptor in a ligand-free form. *J Mol Biol* 416, 629-641.
- Young, S.G., and Zechner, R. (2013). Biochemistry and pathophysiology of intravascular and intracellular lipolysis. *Genes Dev* 27, 459-484.
- Zhao, B., Gandhi, S., Yuan, C., Luo, Z., Li, R., Gårdsvoll, H., de Lorenzi, V., *et al.* (2015). Stabilizing a flexible interdomain hinge region harboring the SMB binding site drives uPAR into its closed conformation. *J Mol Biol* 427, 1389-1403.

TABLES

Table 1

Kinetic rate constants for GPIHBP1 interactions with CTD and LPL homodimers^a

	k_{on} ($10^5 \text{ M}^{-1} \text{ s}^{-1}$)	k_{off} (s^{-1})	K_D (μM)	n	capture
GPIHBP1 ^{1-131/R38G}	10.4 ± 1.9	0.12 ± 0.04	0.12 ± 0.04	11	CTD
GPIHBP1 ¹⁻¹³¹	11.2 ± 4.0	0.22 ± 0.07	0.29 ± 0.13	10	CTD
GPIHBP1 ^{34-131/R38G}	1.0 ± 0.6	0.10 ± 0.01	1.41 ± 0.76	4	CTD
GPIHBP1 ^{1-131/W89S}	nbd	nbd	nbd	2	CTD
GPIHBP1 ^{1-131/R38G} N-gly ^b	10.6	0.16	0.15	2	CTD
GPIHBP1 ^{1-131/R38G}	9.9 ± 5.0	0.023 ± 0.006	0.025 ± 0.007	8	LPL
GPIHBP1 ¹⁻¹³¹	6.5 ± 4.4	0.020 ± 0.007	0.038 ± 0.029	8	LPL
GPIHBP1 ^{34-131/R38G}	1.9 ± 0.4	0.019 ± 0.005	0.091 ± 0.012	4	LPL
GPIHBP1 ^{1-131/R38G}	nbd	nbd	nbd	1	CTD ^{C418Y}
GPIHBP1 ^{34-131/R38G}	nbd	nbd	nbd	1	CTD ^{C418Y}

^aThe kinetic rate constants (k_{on} and k_{off}) were derived by global fitting of sensorgrams obtained by either single-cycle kinetics (LPL) or a mixture of single- and multi-cycle kinetics (the CTD of LPL); the dissociation equilibrium constant K_D was calculated as k_{on}/k_{off} .

^bIntact GPIHBP1^{1-131/R38G} (2 nmols) was incubated overnight at 37°C with 2 U N-glycanase under native conditions. The deglycosylated protein remained monomeric, as judged by analytical size-exclusion chromatography (as performed in Figure 1C).

n , number of separate determinations, each involving a complete set of analyte concentrations analyzed on different days and/or different CM4 chips.

nbd, no specific binding detected

Table 2**Preservation of LPL structure and activity by GPIHBP1 binding**

Added ligand	Unfolding of NTD in LPL (%) ^a	Loss of triolein hydrolase activity (%) ^b	Loss of esterase activity (%) ^b
GPIHBP1 ^{1-131/R38G}	32.6 ± 5.7	28.7 ± 1.5	11.4 ± 6.7
GPIHBP1 ^{34-131/R38G}	79.2 ± 4.2	51.5 ± 1.3	34.7 ± 8.4
GPIHBP1 ¹⁻³³	43.0 ± 5.1	4.2 ± 1.8 ^b	9.8 ± 6.9 ^b
None	100	100	100

^aInhibition of the spontaneous decay of LPL by GPIHBP1¹⁻¹³¹, GPIHBP1³⁴⁻¹³¹, or GPIHBP1¹⁻³³ was measured after a 45-min incubation at 25°C. Equimolar amounts of GPIHBP1 and LPL homodimers were present during the incubation step.

^bTriolein hydrolase activity was measured with a [³H]triolein substrate; esterase activity was measured with a soluble fluorescent substrate. Activity assays were performed on LPL samples that were subjected to the same pre-incubation conditions used for the HDX-MS experiments^a except that *GPIHBP1*¹⁻³³ was present in 5-fold molar excess compared to LPL. The protection by GPIHBP1 variants is shown relative to the decay of LPL after a 45-min incubation without any added binding partner (defined as 100%). Measurements were performed in triplicate.

Figure legends

Figure 1. Model of human GPIHBP1. *Panel A* shows a cartoon representation for glycolipid-anchored human GPIHBP1. Predicted β -sheets are shown in cyan; acidic amino acid residues in the N-terminal domain are highlighted by red sticks; and the consensus disulfide bonds are shown in yellow. *Panel B* shows a “disorder prediction” for human GPIHBP1 sequence based on the IUPred algorithm. Locations of the six strands of the three-fingered-fold of the LU domain are highlighted by boxes (A–F); strands predicted to form β -sheets are colored cyan. *Panel C* documents the homogeneity and monomer status of purified GPIHBP1^{1–131/R38G} (#A) and GPIHBP1^{34–131/R38G} (#B) by analytical size-exclusion chromatography with a Superdex HR75 column operated with 20 mM NaH₂PO₄ and 150 mM NaCl (pH 7.2) and SDS-PAGE (*inset*). Elution positions of the calibration standards are indicated by blue arrows: ovalbumin (43 kDa), carbonic anhydrase (29 kDa), ribonuclease (13 kDa), and aprotinin (6.5 kDa). *Panel D* provides a heat map representation of the relative deuterium uptakes (relative to a fully exchanged control) in peptic peptides from free and LPL-occupied GPIHBP1^{1–131} as assessed by HDX-MS. Deuterium uptake was measured after 10-, 100-, and 1000-sec incubations in D₂O, and relative deuterium uptake is assigned according to the color code (ranging from *blue*, no deuterium uptake, to *red*, full deuterium uptake). A cartoon representation of the differential deuterium uptake for the LU domain between free and LPL-occupied GPIHBP1 after a 10-sec exchange is shown in *panel E*. Shown as sticks are the positions of Thr⁸⁵, Ser⁸⁷, and Trp⁸⁹ in β -strand D of GPIHBP1. Raw deuterium uptake values for peptides 1–21 and 83–109 are shown for free and LPL-occupied GPIHBP1 (*blue* and *red* solid lines, respectively). The dashed line represents a “full deuteration” control.

Figure 2. Mapping GPIHBP1 interaction sites on LPL. Differential deuterium uptake values for free LPL and LPL occupied with intact GPIHBP1^{1–131} (*panel A*) or the acidic domain peptide

GPIHBP1^{1–33} (*panel B*) are shown as butterfly representations. The butterfly plot in *panel C* compares LPL occupied with GPIHBP1^{1–131} or GPIHBP1^{1–33}. Due to inherent instability of LPL homodimers, the deuterium uptake was only examined at 10- (*orange*) and 100-sec (*black*) incubations. The data points represent the mean of triplicate measurements, and the shaded grey area corresponds to the largest S.D. in the data sets recorded for each peptide. A total of 92 peptides were recovered from LPL, and they are numbered consecutively from the N-terminus. The sequences of the individual peptides are found in Figure 2–figure supplement 1B. The transparent red and cyan colors on the left in *panel A* localize peptides to either the N-terminal (NTD) or the C-terminal (CTD) domains of LPL, respectively. *Panel D* shows a cartoon representation of human LPL. Two regions having the most pronounced changes in deuterium uptake with GPIHBP1 binding are highlighted in *green* (residues 279–293) and *blue* (residues 402–419); basic residues are shown as sticks.

Figure 3. Real-time binding kinetics for the interaction between GPIHBP1 and the CTD of human LPL. *Panel A* shows repeat binding of 100 nM of recombinant CTD^{313–448} from human LPL to immobilized mAb 5D2 followed by multi-cycle injections of twofold dilutions of GPIHBP1^{1–131} (black lines). The green line represents a buffer control; the blue line represents a repeat injection of 250 nM GPIHBP1 at the end of the experiment to demonstrate reproducibility. *Panel B* shows equilibrium binding isotherms for the interactions between the immobilized CTD of LPL and GPIHBP1^{1–131} (*blue*), GPIHBP1^{34–131} (*red*), and GPIHBP1^{1–131/W89S} (*green*) with the SPR resonance signal at 380 sec in *panel A* as equilibrium binding level. *Panel C* shows a kinetic evaluation of the double-referenced SPR data for GPIHBP1^{1–131} with a global fit to a 1:1 binding model (fits shown in red). Note there is a slight decay of the binding signal at equilibrium due to a weak ligand-induced dissociation of the CTD from mAb 5D2; this effect translates into dissociation below baseline for the higher concentration of GPIHBP1^{1–131}. These effects were not observed for GPIHBP1^{34–131}.

Figure 4. Kinetic assessment of the GPIHBP1•LPL interaction by single-cycle titration SPR.

The basic principles in the single-cycle kinetic titration are illustrated in *panel A*. Initially, LPL is captured in a noncovalent fashion on the CM4 sensor surface after a 150-sec injection of 200 nM of purified LPL across the flow cell containing immobilized mAb 5D2. After a 600-sec stabilization period, a series of five 90-sec pulses with increasing analyte concentration are injected without intervening regeneration. The following concentrations of either mAb 4-1a (A), mAb 5D2 (A), GPIHBP1¹⁻¹³¹ (B), or GPIHBP1³⁴⁻¹³¹ (C) were analyzed: 12.5, 25, 50, 100, and 200 nM. *Panels B* and *C* shows the buffer referenced sensorgrams recorded for GPIHBP1¹⁻¹³¹ and GPIHBP1³⁴⁻¹³¹, respectively. The mathematical fitting to a simple 1:1 binding model are superimposed as *red* lines and the residuals are shown in *green*.

Figure 5. Equilibrium binding constants of the GPIHBP1•LPL interaction by microscale thermophoresis.

The microscale thermophoresis signals for the interaction of LPL with 5 nM Alexa Flour-647-labeled GPIHBP1^{1-131/R38G} (*panel A*) and GPIHBP1^{34-131/R38G} (*panel B*) were recorded in quadruplicates for two-fold dilution series of unlabeled LPL₂ (10 pM to 350 nM). The mean values and S.D. for the thermophoresis are shown as well as a fitting to a 1:1 binding model (software supplied with Monolith NT.115).

Figure 6. Progressive unfolding of LPL as determined by HDX-MS.

Panel A shows the unfolding of the catalytic domain of LPL when incubated at 25°C. The unfolding is evident from the appearance of a bimodal isotopic envelope for the peptide 131–165, which contains Ser¹³⁴ and Asp¹⁵⁸ of the catalytic triad. *Panel B* shows the global distribution of peptides in the catalytic domain that undergo unfolding (in *red*). The peptide 131–165 is highlighted in *yellow*. Peptides that are not exhibiting bimodal isotope envelopes are colored *light blue*; segments of LPL not recovered by the HDX-MS are colored *grey*. The impact of GPIHBP1¹⁻¹³¹ and the N-terminal acidic peptide GPIHBP1¹⁻³³ on

LPL unfolding is shown in *panel C*. In these studies, equimolar amounts of GPIHBP1¹⁻¹³¹ or GPIHBP1¹⁻³³ (relative to the LPL₂) inhibited unfolding of the NTD of LPL. The progressive unfolding of LPL was quantified by fitting two Gaussian distributions to the isotopic envelopes of peptide 131–165 representing the folded and unfolded states (*panel A*) and is shown in *panel D* (*black circles*). Unfolding at the 45-min incubation time point was measured in triplicates with and without equimolar amounts of GPIHBP1¹⁻¹³¹ (*green circle*) or GPIHBP1¹⁻³³ (*red circle*). The progressive loss of triolein hydrolase and esterase activities of LPL were recorded in parallel as a time-dependent function of pre-incubating 2 μ M LPL₂ under identical conditions and is shown by the *yellow squares* and *blue triangles*, respectively.

Figure 7. Zero-length cross-linking of GPIHBP1¹⁻¹³¹ and GPIHBP1¹⁻³³ to bovine LPL. *Panel A*, left shows a Coomassie Blue–stained 12% polyacrylamide gel after SDS-PAGE analysis of reduced and alkylated samples representing various combinations of 1.5 μ M LPL₂ and 7 μ M GPIHBP1 variants subjected to EDC cross-linking. *Lane 2* shows LPL + GPIHBP1¹⁻¹³¹ before cross-linking. Lanes 3–6 show samples after EDC cross-linking: GPIHBP1¹⁻¹³¹ (*lane 3*); LPL (*lane 4*), LPL + GPIHBP1¹⁻¹³¹ (*lane 5*), and LPL + GPIHBP1³⁴⁻¹³¹ (*lane 6*). The covalently bound conjugate representing LPL•GPIHBP1¹⁻¹³¹ is marked by an asterisk. *Right panel* shows a Coomassie Blue–stained 4–12% gradient polyacrylamide gel after analysis of EDC cross-linked 3 μ M LPL₂ alone (*lane 8*) or in the presence of 15 μ M GPIHBP1¹⁻³³ (*lane 9*); 15 μ M GPIHBP1³⁴⁻¹³¹ (*lane 10*); and 15 μ M GPIHBP1¹⁻¹³¹ (*lane 11*). The covalent conjugates representing LPL•GPIHBP1¹⁻¹³¹ and LPL•GPIHBP1¹⁻³³ are indicated by an asterisk and a solid dot, respectively. Molecular weight markers are shown in *lanes 1, 7 & 12*. *Panel B* shows a model of human LPL highlighting the cross-linking sites in GPIHBP1 that were identified by MS (*asterisks*). Areas that have been assigned as potential interaction sites for GPIHBP1 by HDX-MS are shown in *green* (for the acidic domain of GPIHBP1) and *blue* (for the LU domain of GPIHBP1). The position of the interdomain interface in

LPL between the NTD and CTD is marked by a dashed line, and three residues within this interface linked to familial chylomicronemia when mutated (S259R, G409R, and E410V) are shown by grey numbers. Basic residues of the heparin-binding site in the catalytic domain of LPL (R279, K280, R282) are shown as sticks. Note, bovine LPL contains two additional residues compared to human LPL *e.g.* Lys²⁹⁶ in human LPL is equivalent to Lys²⁹⁸ in bovine LPL.

Figure 1–figure supplement 1

Constructs encoding soluble DIII-ent-hGPIHBP1^{1–131/R38G} and DIII-ent-hLPL^{313–438}. Schematic representation of the vectors used for *Drosophila* S2 cell expression of a soluble, secreted human GPIHBP1^{1–131} (*panel A*) and the CTD^{313–448} of human LPL (*panel B*). Both constructs use the third LU domain from human uPAR (DIII^{192–283}) as an N-terminal purification tag as described (Gårdsvoll et al., 2013). The enterokinase cleavage site used to excise the recombinant protein (and remove the uPAR tag) is highlighted in black. *pMT* and *BiP* represent the *Drosophila* metallothionein promoter and secretion signals, respectively. To optimize enterokinase-mediated excision of GPIHBP1, two mutations (DIII^{R281G} and GPIHBP1^{R38G}) were introduced to silence two undesired cleavage sites for enterokinase. In the GPIHBP1 construct, the N-terminal signal peptide and the C-terminal hydrophobic peptide required for glycolipid anchoring have been omitted.

Figure 1–figure supplement 2

Purification of recombinant soluble human GPIHBP1^{1–131/R38G} and GPIHBP1^{34–131/R38G}. *Panel A* shows a cation-exchange chromatography elution profile for 30 mg of purified DIII-ent-GPIHBP1^{1–131/R38G} after enterokinase cleavage. We used a 5 ml HiTrap SP FF column and a 35-ml linear gradient from 0 to 1.0 M NaCl in 50 mM CH₃COOH, pH 4.5. The peaks correspond to: intact GPIHBP1^{1–131/R38G} (#A), GPIHBP1^{34–131/R38G} (#B), uncleaved fusion protein (#C) and the excised uPAR DIII tag

(#D), as judged by SDS-PAGE of reduced and alkylated samples (*panel B*) and mass spectrometry (not shown).

Figure 1—figure supplement 3

Comparison of the dynamics in GPIHBP1^{34–131} and GPIHBP1^{1–131} in HDX-MS experiments.

Differential deuterium uptake between intact GPIHBP1^{1–131} and GPIHBP1^{34–131} (a truncated GPIHBP1 lacking the N-terminal acidic domain) measured by HDX-MS at 25°C is shown as a butterfly plot. Deuterium uptake was traced for 10- (*orange*), 100- (*black*), and 1000-sec (*blue*). The shaded grey area corresponds to the largest S.D. of the data sets recorded for each peptide. Data points represent the mean of triplicate measurements.

Figure 1—figure supplement 4

Peptide list for pepsin-treated GPIHBP1. Peptides recovered after HDX and pepsin cleavage of recombinant human GPIHBP1 are shown as blue bars.

Figure 2—figure supplement 1

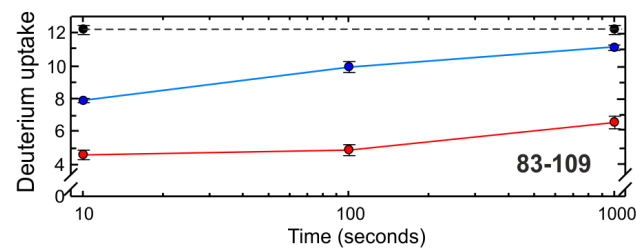
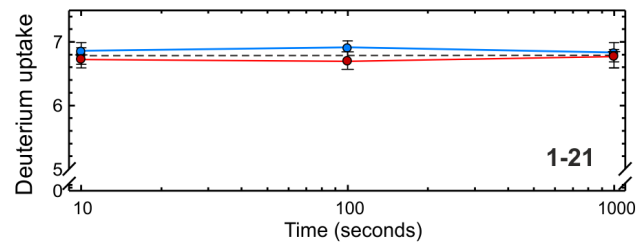
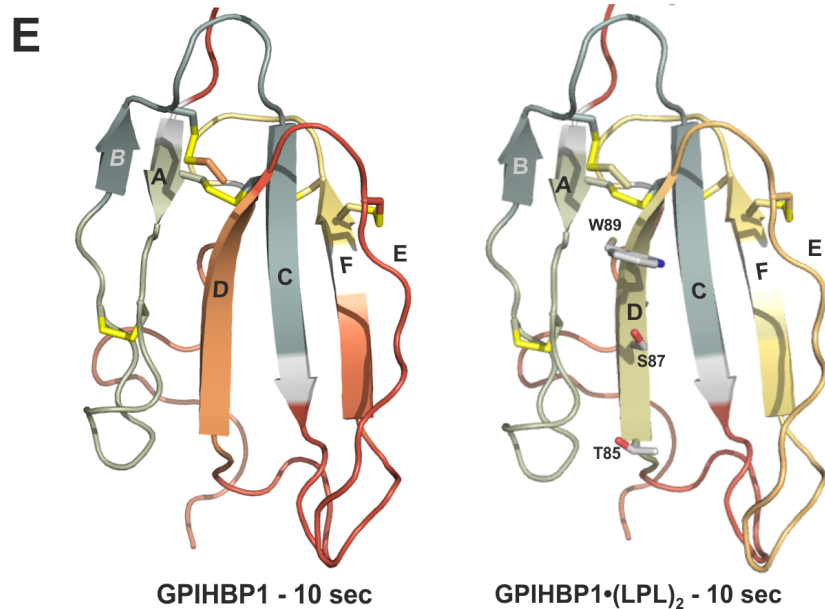
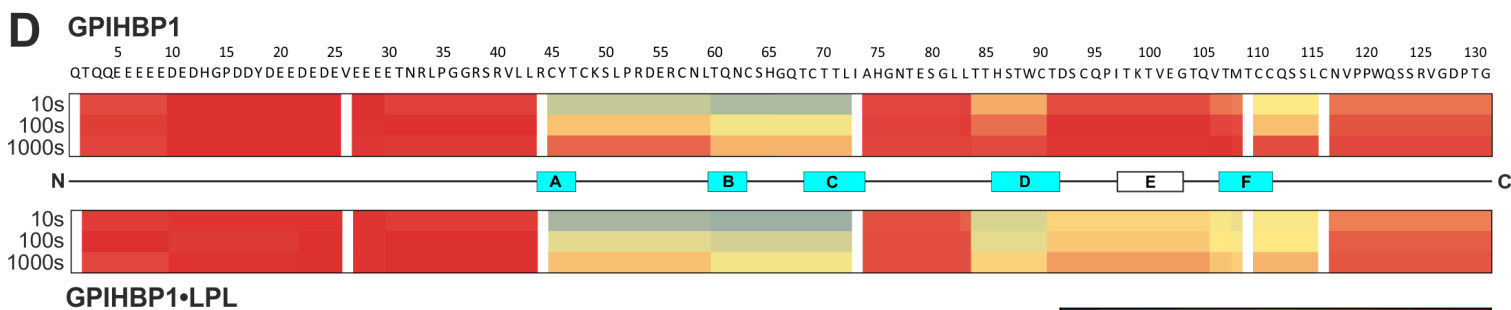
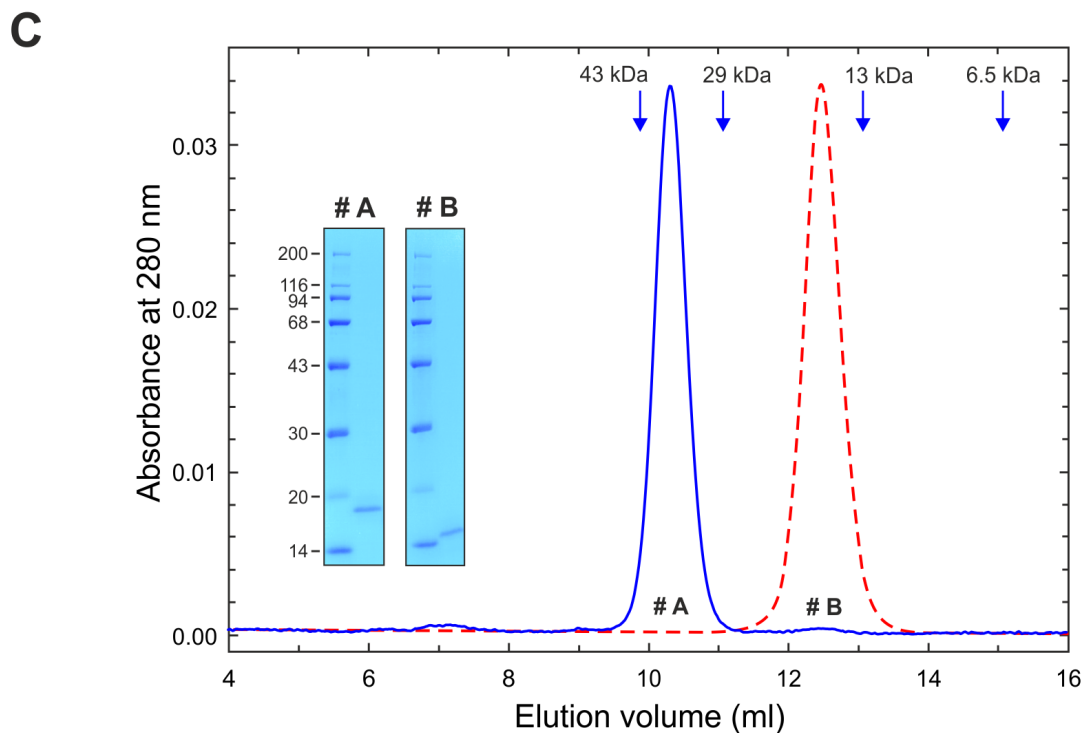
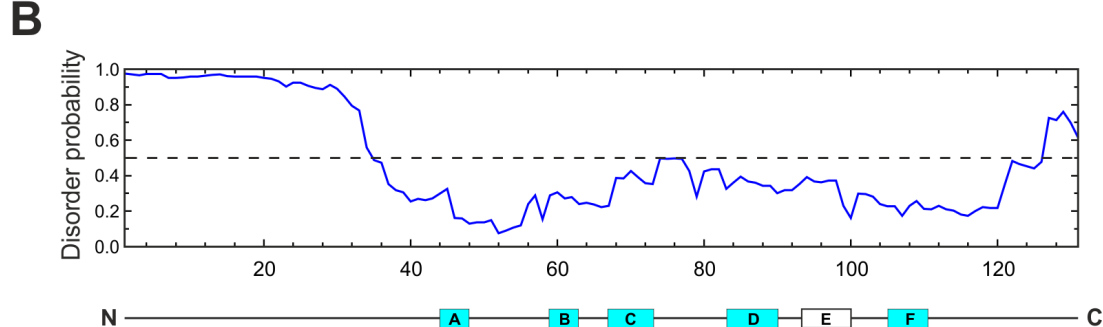
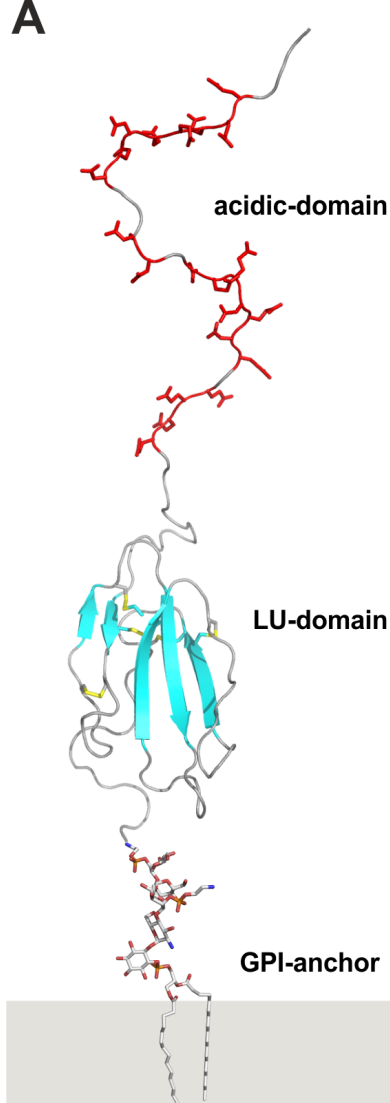
Peptide list for pepsin-treated bovine LPL. *Panel A* shows peptides recovered in the HDX-MS studies. Peptides recovered from bovine LPL after pepsin cleavage are shown as blue bars. The CTD is highlighted by the transparent light green box; N-linked glycosylation sites are shown (CHO); residues forming the catalytic triad are indicated by blue asterisks; heparin-binding sequences are shown by green asterisks. *Panel B* shows the inventory of 92 peptides recovered from LPL. Peptides designated with an asterisk display a bimodality of their isotopic envelopes after a 45-min incubation in H₂O-buffers followed by 10- and 100-sec incubations in D₂O buffers (as illustrated for the peptic peptide 131–165 in Figure 6A).

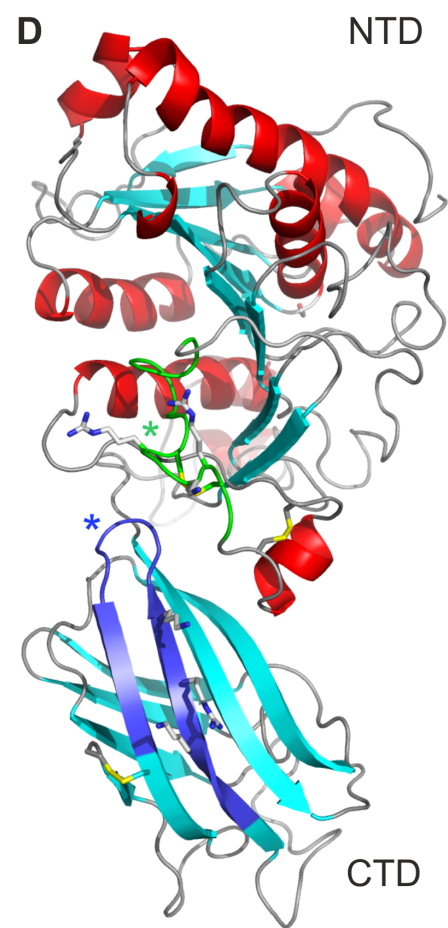
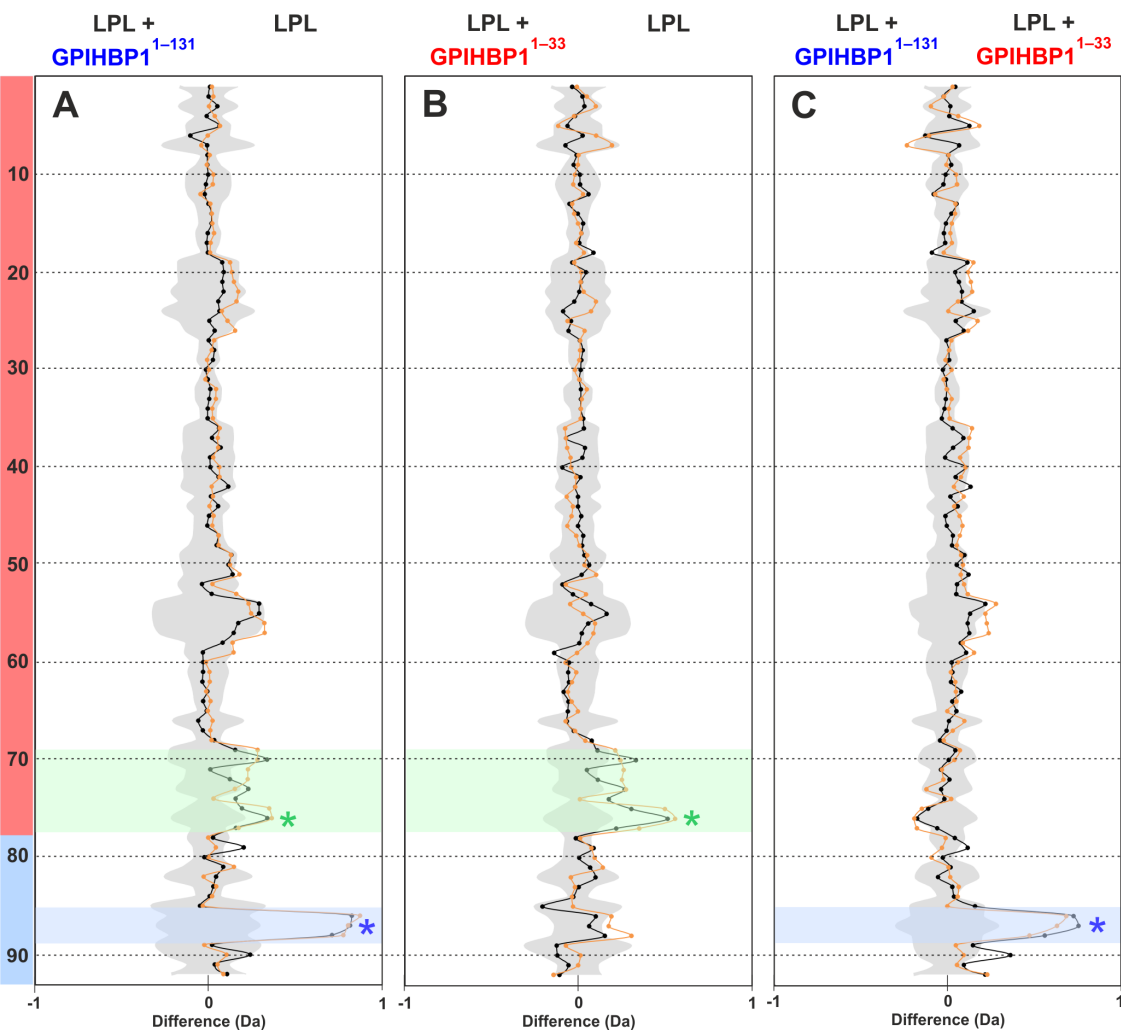
Figure 7—figure supplement 1

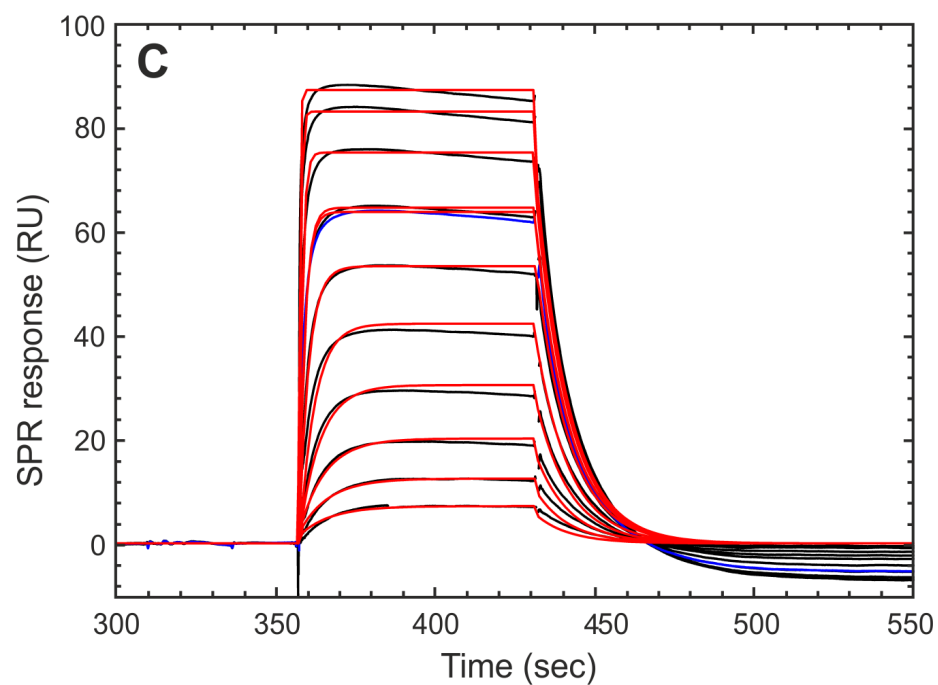
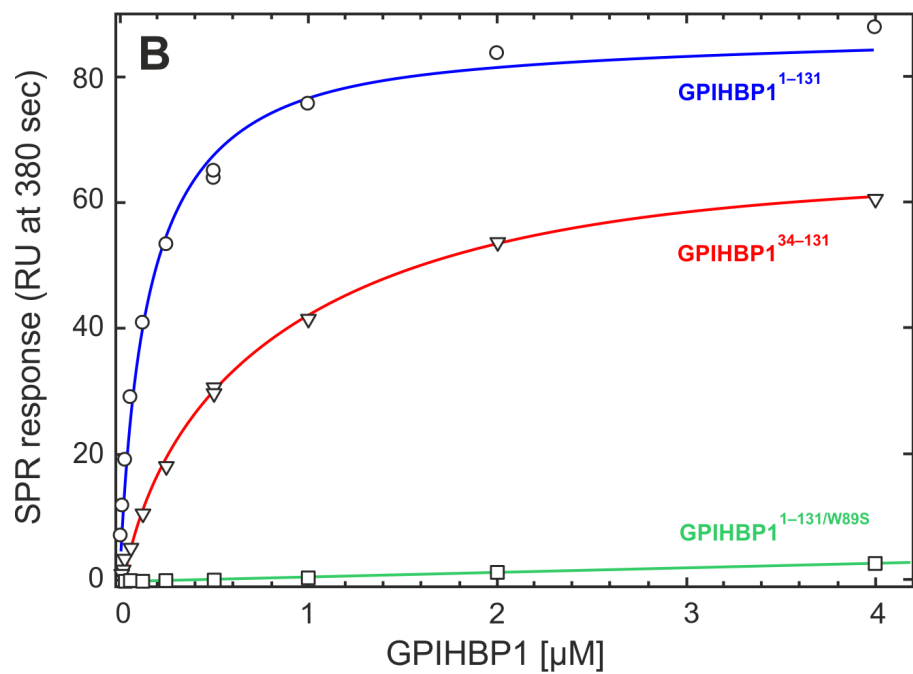
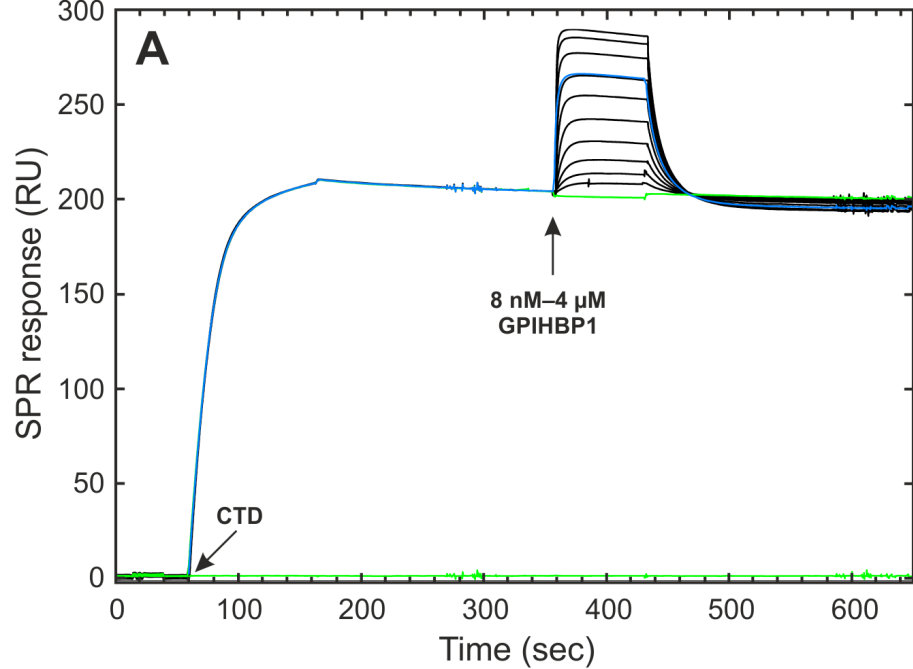
Fragment spectra identifying EDC-mediated inter-domain cross-links in mature LPL•GPIHBP1¹⁻¹³¹ complexes. *Panel A* shows the fragment spectra produced for the EDC cross-linked peptide between residues 1–33 in GPIHBP1 and residues 295–299 (VARKR) in bovine LPL. *Panel B* shows the fragment spectra produced for the cross-linked peptide between residues 1–33 in GPIHBP1 and residues 416–422 (KVIFCSR) in bovine LPL. Fragments derived from residues 1–33 of GPIHBP1 are designated (*A*) and peptides from LPL are designated (*B*). The *blue peaks* correspond to y-fragment ions from either peptide; *green peaks* correspond to b-fragments ions from either peptide; *red peaks* represent unassigned peaks; *purple peaks* correspond to loss of NH₃ or H₂O (not labeled) or ions that have undergone two fragmentation reactions. Peaks corresponding to cross-linked peptide fragments are assigned by an × along with the two peptide fragments (*e.g.*, DEDH×KR).

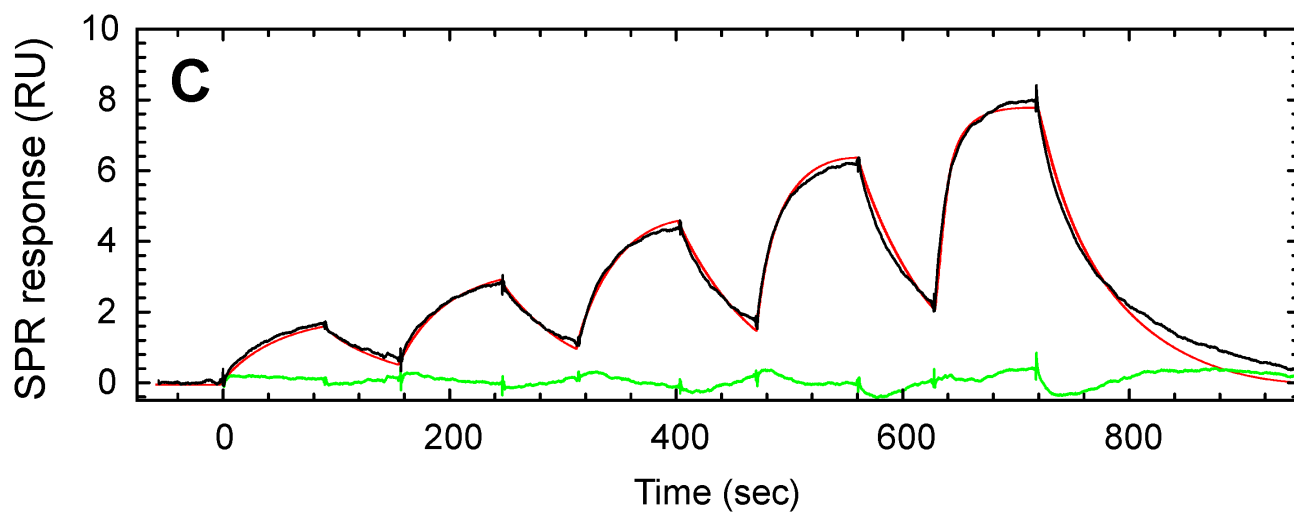
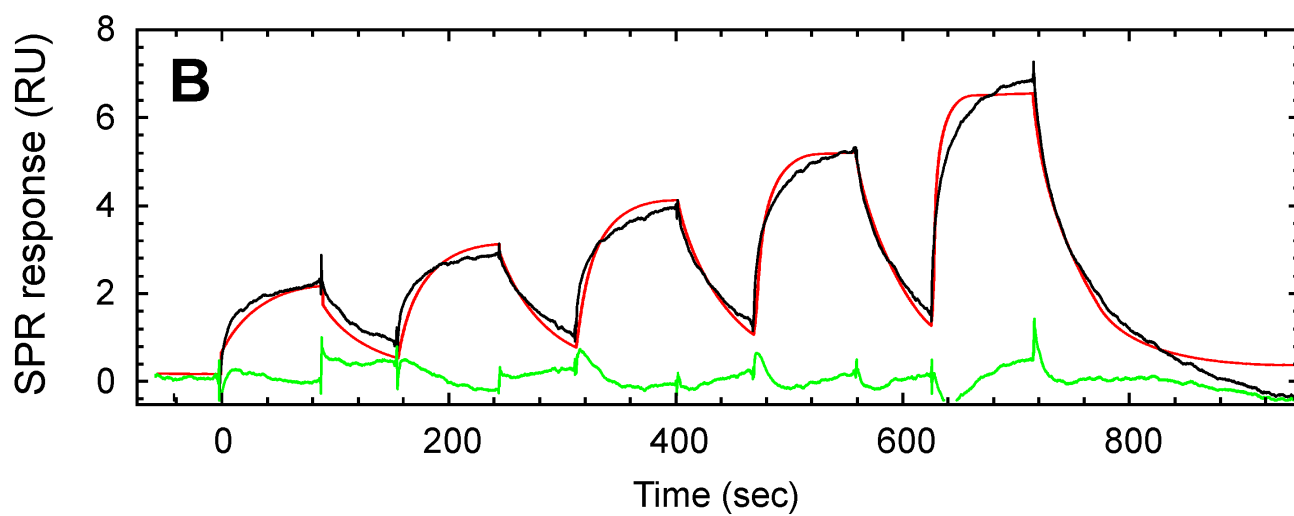
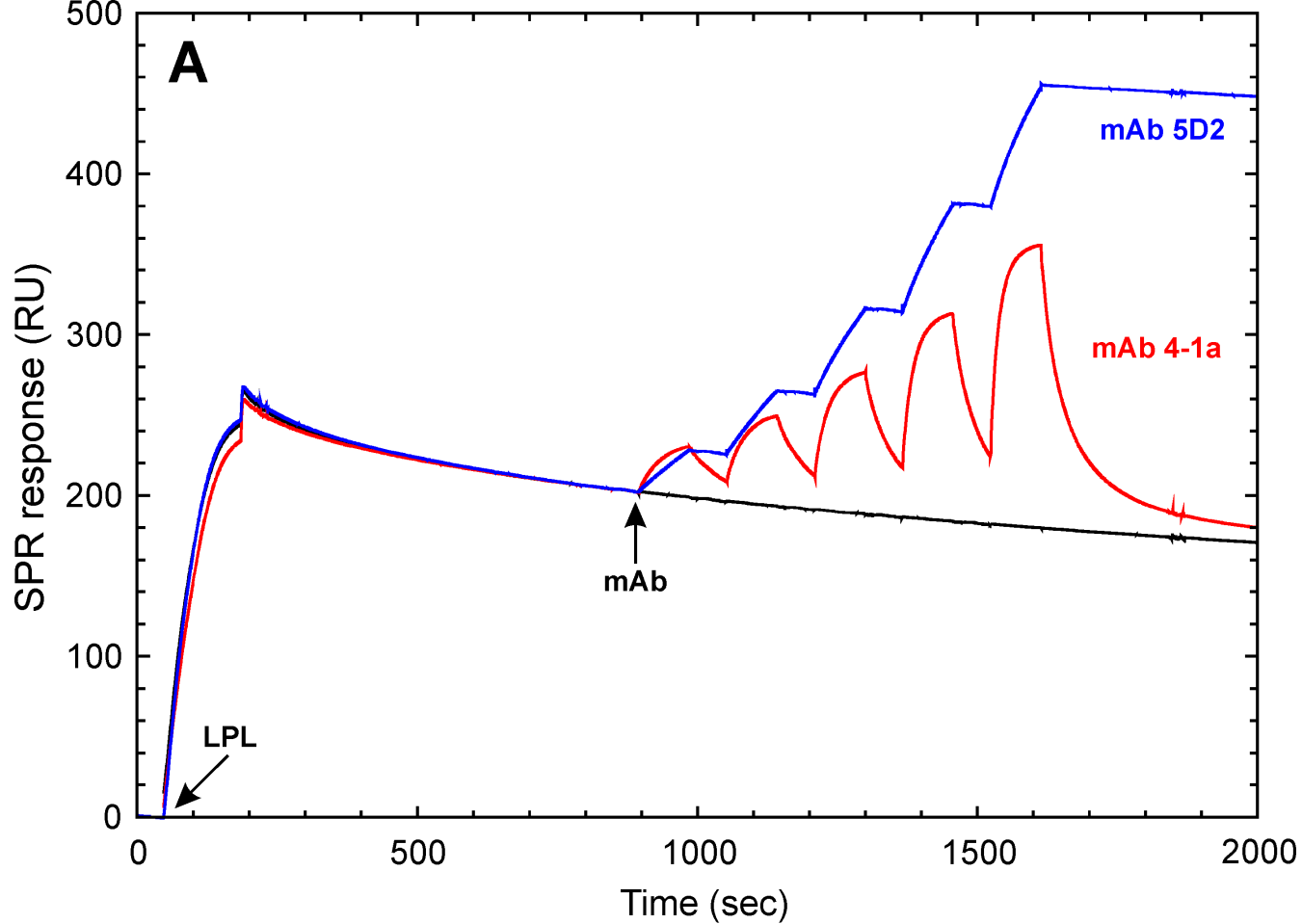
Figure 7—figure supplement 2

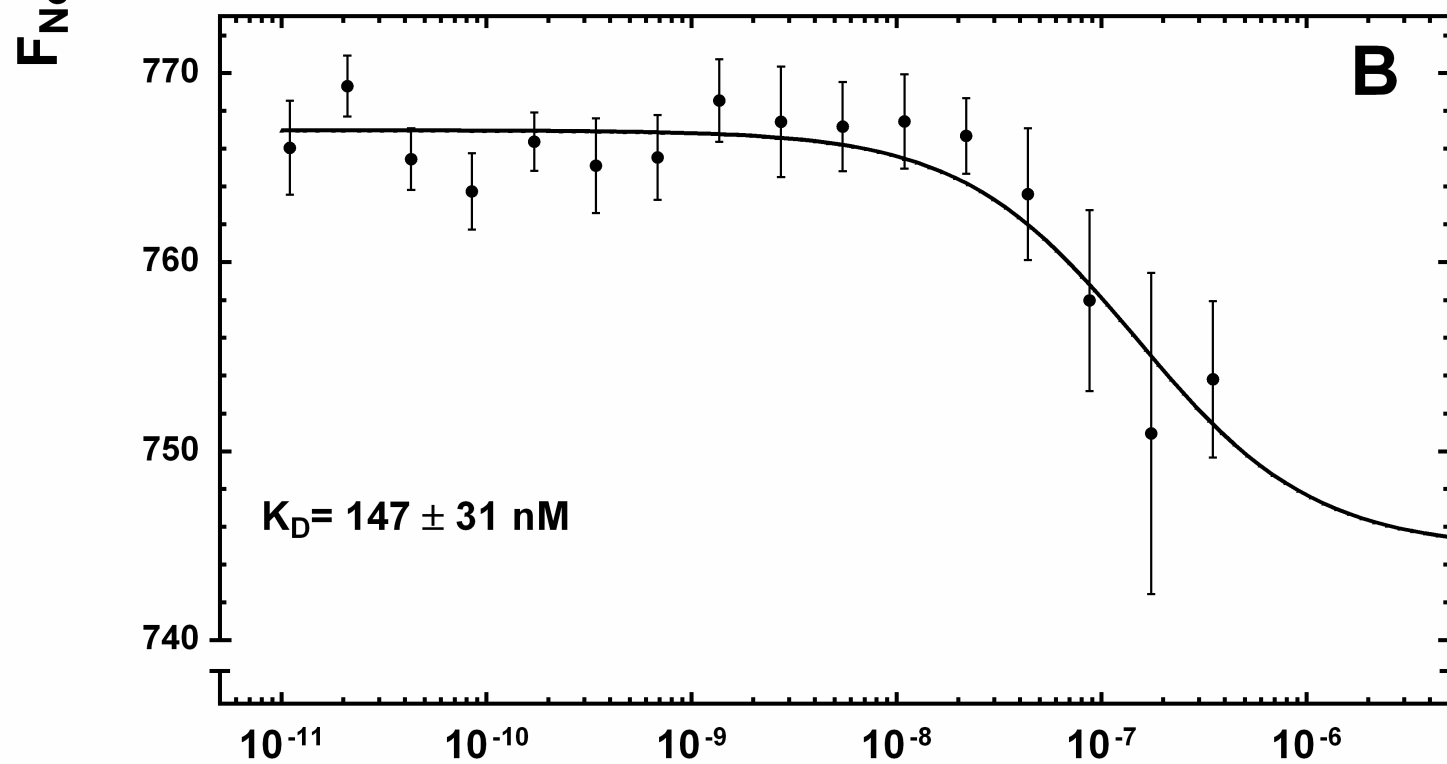
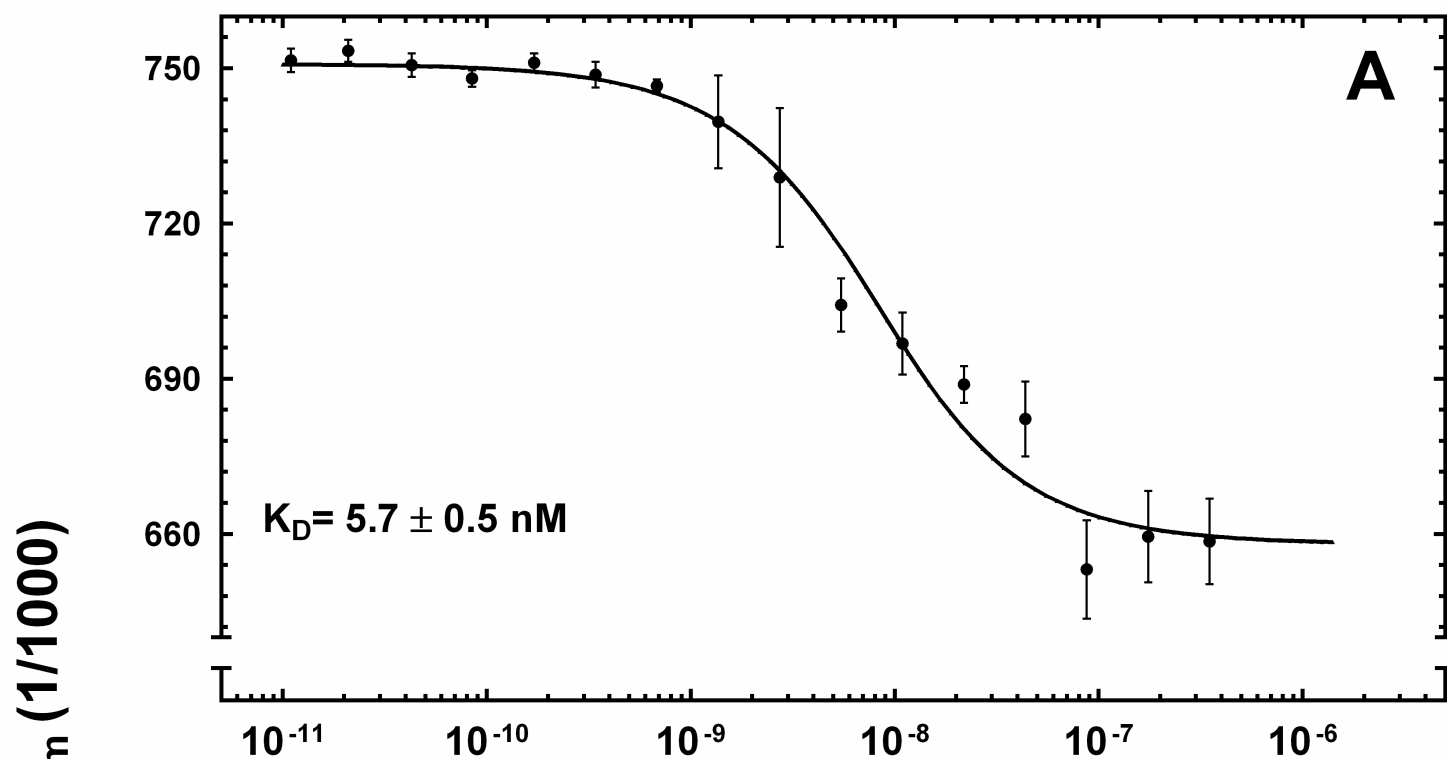
SDS-PAGE analysis of EDC/NHS cross-linked LPL•GPIHBP1 complexes. The cross-linking efficiencies between LPL and GPIHBP1³⁴⁻¹³¹ or GPIHBP1¹⁻¹³¹ are revealed by a Coomassie Blue–stained 12 % SDS-polyacrylamide gel. The samples were cross-linked for 4 h by 5 mM EDC and 5 mM NHS in the following format: 3 μM LPL₂ alone (*lane 3*) or in the presence of 15 μM GPIHBP1³⁴⁻¹³¹ (*lane 4*) or 15 μM GPIHBP1¹⁻¹³¹ (*lane 5*). LPL without EDC/NHS is shown in *lane 2*. Molecular mass markers are in *lane 1*. The asterisk shows a covalent LPL•GPIHBP1³⁴⁻¹³¹ conjugate. Using these cross-linking conditions, we observe a low level of covalently-linked LPL dimers (*lane 3*); the amount of these LPL dimers is reduced by the presence of GPIHBP1³⁴⁻¹³¹ or GPIHBP1¹⁻¹³¹ (*lane 4 & lane 5*), likely reflecting the engagement of LPL in interactions with these ligands.



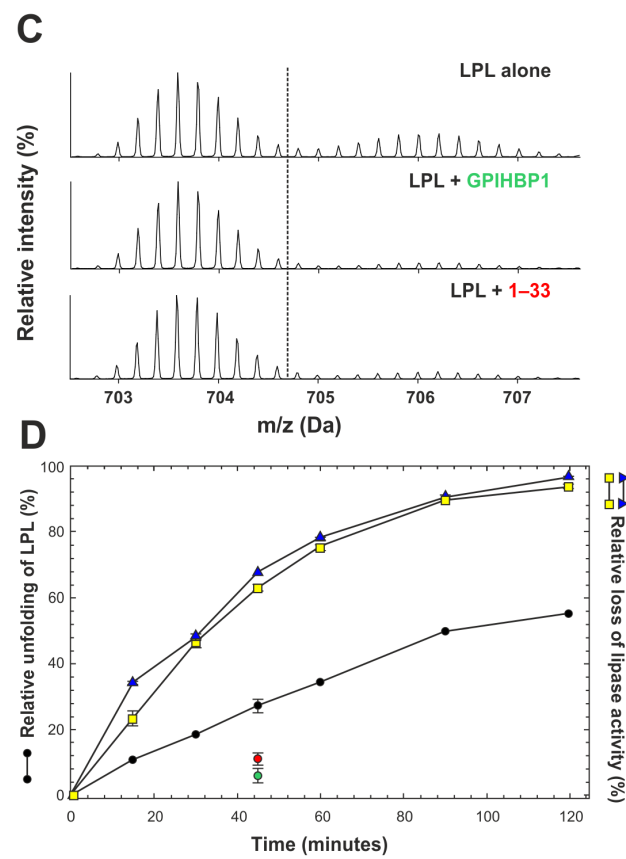
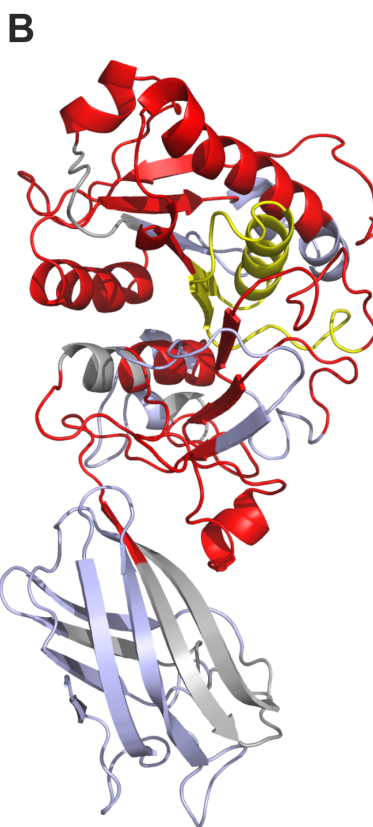
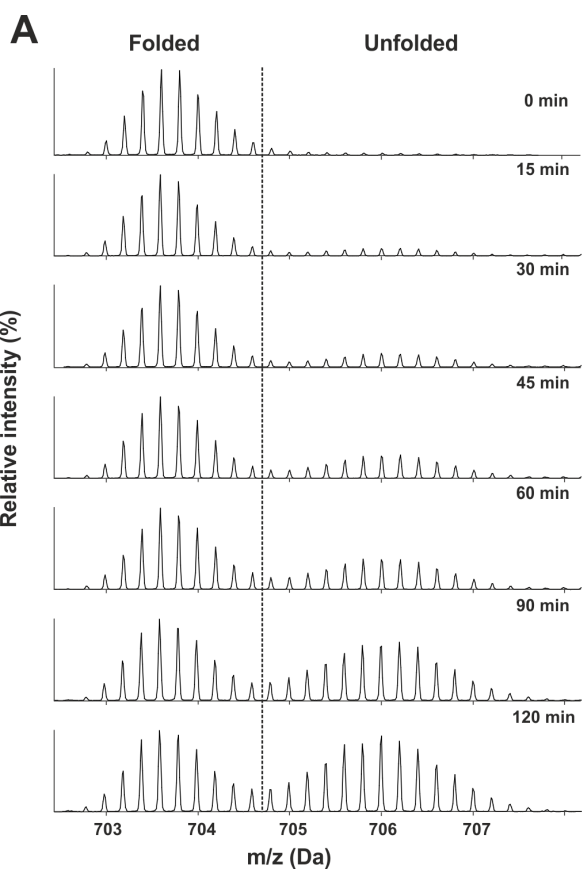


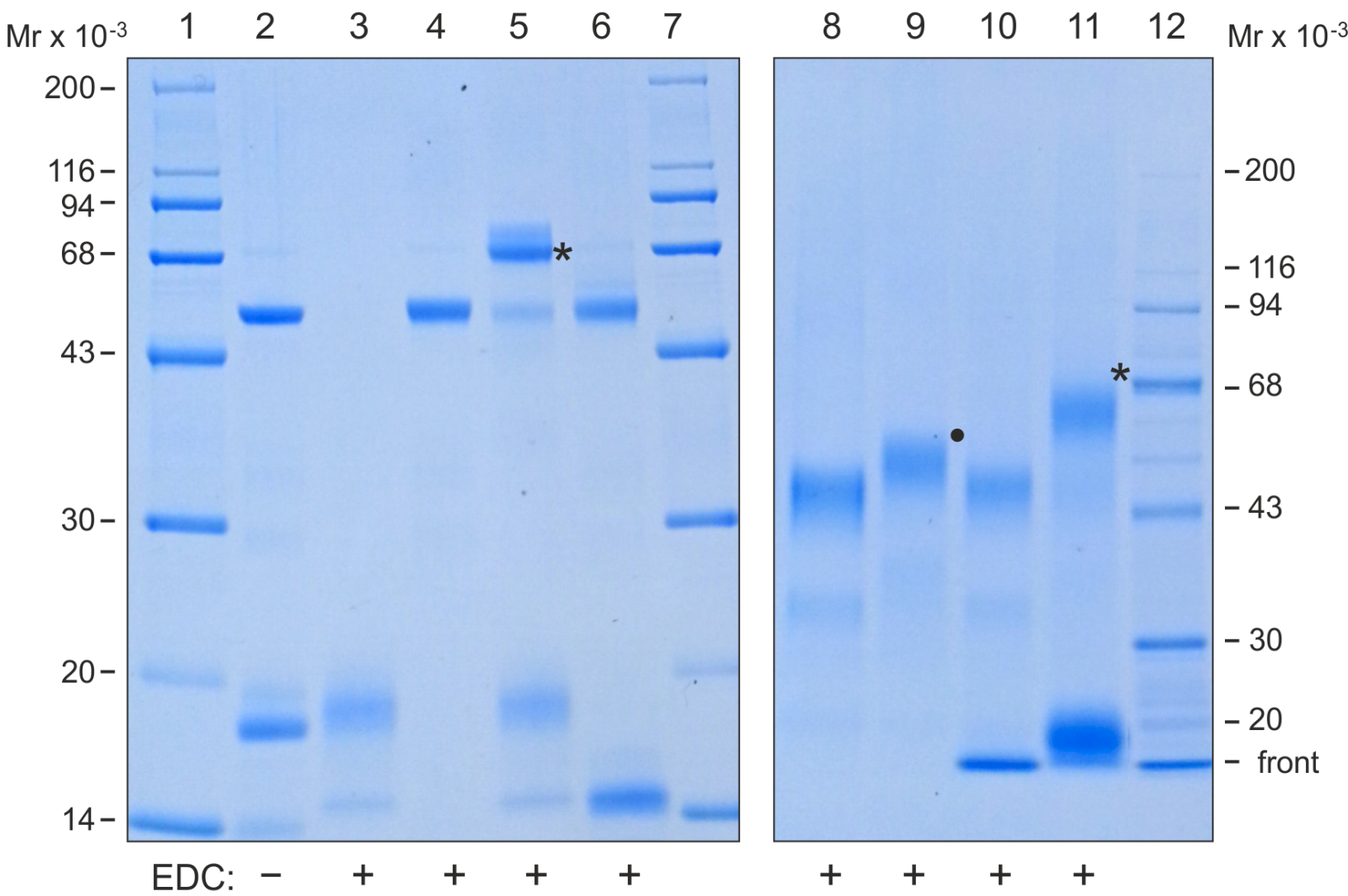






Concentration of LPL₂ (M)



A**B**